The completion of this thesis
was supported by the
**Randy Seeling Award**
given, in his memory, to another
outstanding graduate student
of the Geology Department,
University of Minnesota, Duluth.

# SUBAQUEOUS PYROCLASTIC VOLCANISM IN THE VICINITY OF THE HELEN MINE, WAWA, ONTARIO

A THESIS

SUBMITTED TO THE FACULTY OF THE GRADUATE SCHOOL

OF THE UNIVERSITY OF MINNESOTA

BY

MARK WARREN OSTERBERG

IN PARTIAL FULFILLMENT OF THE REQUIREMENTS

FOR THE DEGREE OF

MASTER OF SCIENCE

DECEMBER 1982

## ABSTRACT

A superbly exposed and preserved succession of felsic subaqueous (partially subaerial) pyroclastic flow deposits and related hydroclastic rocks are exposed stratigraphically below the Helen Iron Formation near Wawa, Ontario. This succession is located in the Abitibi-Michipicoten greenstone belt and is regionally associated with volcanogenic iron formation, pillowed mafic flows, and volcaniclastic sedimentary rocks. The metamorphic grade is lower greenschist facies.

Felsic volcanism began with the emplacement of finely bedded, poorly sorted, fragmented hydroclastic rhyolites produced by phreato-magmatic explosions. The hydroclastic rocks pass stratigraphically upward into bedded pyroclastic flow deposits which are overlain in turn by finely bedded ash deposits. This sequence is repeated at least twice and is then overlain by crystal tuffs and contemporaneous pumice-bearing tuffs. The pumice-bearing tuffs are thought to be segregated from the crystal tuffs by the different settling rates of crystals and pumice through a water column. The top of the pumice-bearing tuffs marks the end of the first cycle of felsic volcanism. Interbedded with the pumice-bearing and crystal tuffs are chlorite rich dacite and/or andesite pillow breccia, amygdaloidal flows, and/or subvolcanic intrusions, and accessory bearing, lithic rich pyroclastic flow deposits. Stratigraphically above the andesites occurs a second cycle of felsic volcanism marked by the sequence hydroclastic rocks, crystal tuffs, and pumice-bearing tuffs. The upper portion of the second cycle is capped and/or intruded by massive, flow laminated, and spherulitic rhyolitic domes and/or lava flows.

The domes and/or lava flows are surrounded by rhyolitic, coarse, poorly sorted, chaotic block and ash size volcanic breccias that are thought to be related genetically to the domes and/or lava flows. The block and ash deposits are in turn surrounded by well sorted, lapilli and ash deposits. Iron formation consisting of an upper banded chert member, a middle massive pyrite member, and a lower massive siderite member is located stratigraphically above the felsic volcanics and below the pillowed mafic flows. It is associated with an alteration zone in the footwall rhyolites marked by the presence of chloritoid, epidote, chlorite, and stilpnomilane stringers. Four ages of mafic dikes at the footwall felsic volcanics, iron formation, and pillowed mafic volcanics.

Whole rock and trace element chemical analyses of representative samples showed subalkaline trends and confirmed the rhyolitic and dacitic field identifications of rocks from the area. The raw chemical data was corrected for metasomatism after the method of Beswick and Soucie (1978). This procedure identified $SO_2$, FeO + MgO, CaO, $Na_2O$, and $K_2O$ as mobile constituents during post volcanic modification of original compositions.

The eruption cycle is thought to have begun with short lived, subaqueous, phreatomagmatic activity, changing with time to a sustained eruption column that may have been subaqueous and/or subaerial. After two such cycles, rhyolitic domes and/or lava flows with associated Merapi-type pyroclastic flows capped with pyroclastic deposits. The last vestiges of felsic volcanism in the area was the fumerolic and hot spring activity that resulted in the alteration of the footwall volcanics and in the deposition of the Helen Iron Formation.

TABLE OF CONTENTS

# LIST OF FIGURES



# LIST OF TABLES

# LIST OF PLATES

# I: INTRODUCTION

## I.1 Purpose of Study

The association of intermediate to felsic pyroclastic rock with Archean massive sulfide deposits has been noted over the years by many geologists (e.g., Sangster, 1972) yet it is only within the last few years that attempts have been made to study these rocks with the intention of determining the nature of the volcanic eruptions that produced them.

This project was undertaken to study the volcanology of the well preserved and exposed felsic volcanic succession which underlies the Helen Iron Formation, a part of the Michipicoten greenstone belt, in northwestern Ontario. The objectives of the study are as follows:

1) to map the felsic volcanic rocks and determine compositions, deposit types, stratigraphy, environments of deposition, and facies changes in part of a relatively undeformed, well preserved Archean greenstone complex
2) to study the post-volcanic changes in the Helen Iron Range footwall rocks
3) to study possible chemical and spacial relationships between the Helen Iron Formation and the felsic footwall volcanics
4) to chemically classify the lithologic units using standard classification criteria and to define any geochemical zonation within the felsic pyroclastic units.

## I.2 Location, Access, and Physiography

The study area is located approximately twelve km inland from the northeast shore of Lake Superior, near the town of Wawa in the Michipicoten district of Ontario, approximately 225 km north-northwest of Sault Ste. Marie (Figure 1). The study area can be reached by taking Highway 17 from either Thunder Bay or Sault Ste. Marie to Wawa. Specific access to the area can be gained by mine roads of the Helen Iron Mine located just north of the Wawa town limits. The map area covers approximately six square km.

Topography in the Michipicoten district is hilly. The maximum elevation in the district, found on the Helen Iron Range, is about 350 meters above the level of Lake Superior. The relief in the map area is approximately 110 meters from the top of the Helen Iron Range to the level of the surrounding countryside. The region is well drained with few swampy areas.

Bedrock exposure in much of the map area approaches 100% due to years of operation of the Algoma Steel Corporation sinter plant that has created an unvegetated and eroded "kill" area approximately 50 km long by 20 km wide to the northeast of the plant (Figure 1). Away from the fumigated "kill" area exposure varies from nil to 60% due to variable amounts of glacial drift supporting a thick cover of deciduous and coniferous vegetation.

## I.3 Methods of Study

This study included field mapping and sampling, petrographic analyses of 110 thin sections, and chemical analyses of thirty-two selected samples for whole rock and trace element composition.

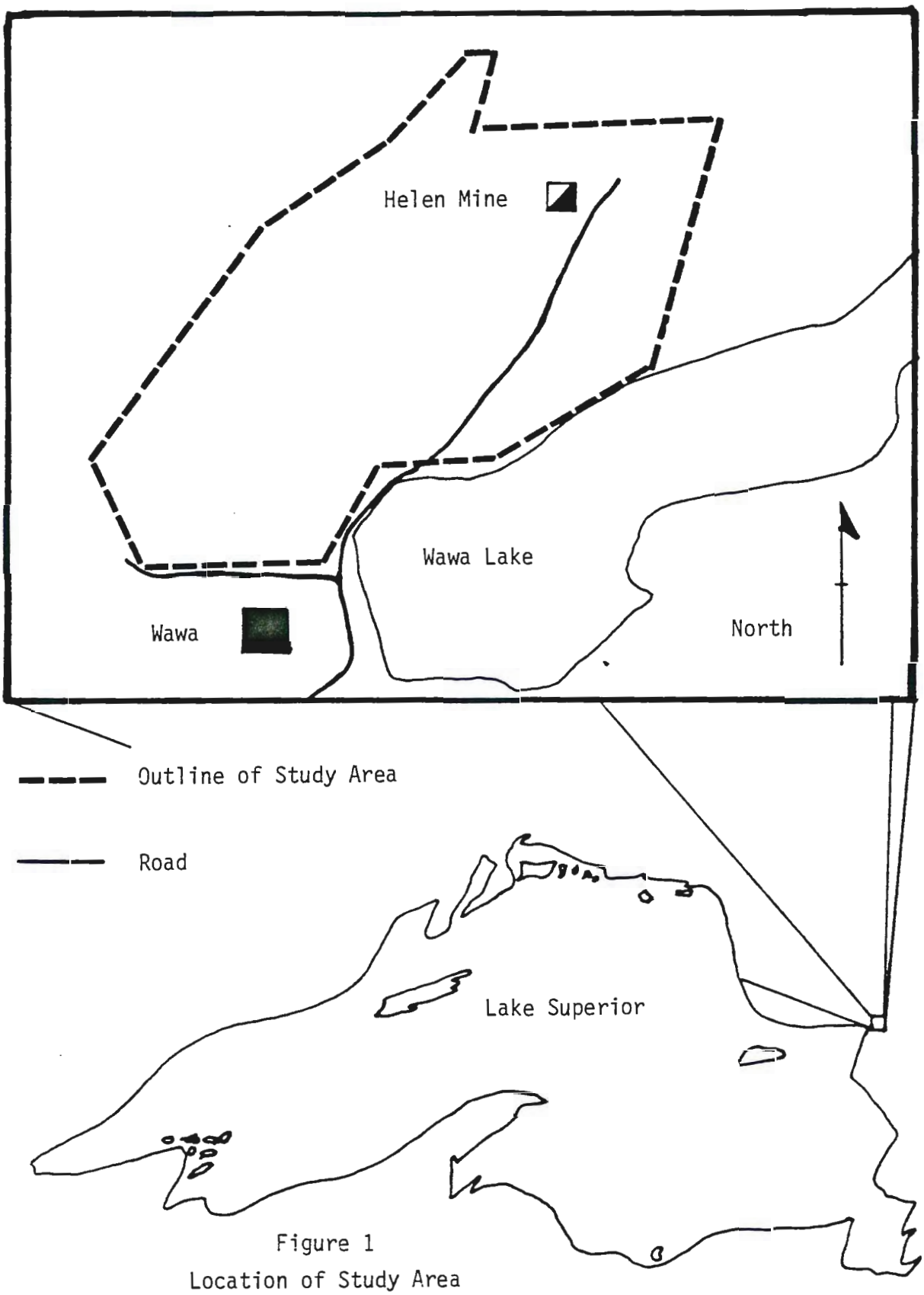


Figure 1
Location of Study Area

The field mapping and sampling was completed in a six week period during June and July of 1980. The mapping was done on mylar overlays of airphotos at one inch to one quarter mile, and on mylar overlays of airphotos at one inch equals 400 feet. Data was transferred to one inch equals 400 feet base maps (Figure 3).

One hundred and ten thin sections were studied for mineral identification and textural analyses to determine original lithologies, extent of alteration, and the degree of metamorphism. Modes and textures of representative samples are listed in Appendix I.

Twenty-five samples were sent to Technical Service Laboratories of Mississauga, Ontario, for whole rock and trace element analyses. The results of the chemical analyses are included in Appendix II. The author also had available data from an additional seven whole rock chemical analyses for samples collected by Algoma Exploration within or near the limits of the study area.

Five thin sections were studied using x-ray diffraction methods to identify the carbonate mineral present.

## I.4 Previous Work

There has been an impressive amount of geologic work accomplished in the Michipicoten district since the iron mines were opened in the late 19th century. Coleman and Willmott (1902) classified the Michipicoten rocks into upper Huronian felsic and mafic volcanics and conglomerates, lower Huronian slates, iron formation, tuffs, greenstones and Laurentian

gneisses and granites. The authors thought the lower Huronian greenstones underlay the tuffs in an eastpitching syncline enclosing rocks of the Helen Iron Range.

Collins and Quirke (1926) separated the Michipicoten rocks into four groups. They assigned the glacial deposits to the Pleistocene, the diabase dikes to the Keweenawan, the granite to the preKeweenawan-postKeewatin, and the Doré sediments, post- and pre-Doré volcanics, and the iron formations to the Keewatin. The authors divided the iron formations into three members: an upper banded chert member, a middle pyrite member, and a lower siderite member.

Grout (1926) reviewed Collins and Quirke's (1926) paper and made the suggestion that the chert member of the iron formation was not deposited contemporaneously with the pyrite and siderite members but that it was deposited first and then acted as an impermeable barrier that channeled the altering solutions through the footwall tuffs replacing them with the pyrite and siderite members.

Gledhill (1927) assigned the diabase dikes to Keweenawan time and the granites and gneisses to Algoman time. He also separated younger Doré sediments from the Keewatin mafic flows, fragmental volcanics, and iron formation. Gledhill concluded that the major axes of folding in the district trended east-west.

Moore (1931) thought the felsic volcanic rocks in the Michipicoten area were much like the felsic volcanic rocks found in other Keewatin areas. He noted that the iron formation occurred between the felsic volcanics below and the mafic volcanics above.

Moore and Armstrong (1946) assigned the diabase dikes to the Keweenawan, lamprophyre dikes to the Algoman, gabbro and diabase intrusions to the Huronian, and the mafic volcanics, felsic volcanics, and iron formation to the Keewatin. They interpreted the sequence as one limb of a tightly compressed anticline slightly overturned to the north. The authors described several large faults and noted that the Helen Mine geologists had located six thrust faults in the orebody with tens to hundreds of feet of movement.

Marsden (1948) in a Jalore company report described the Mildred range in the Michipicoten district as being similar to the other Michipicoten iron ranges. The Mildred Iron Formation consists of a banded chert member bounded on the south by felsic volcanic rocks and on the north by mafic volcanic rocks, quartz-feldspar porphyries, conglomerates, and slates. Marsden described the structure of the Mildred Iron Range as being an isoclinal syncline.

Moore (1948) believed the iron formations and the volcanic rocks of the district to be Keewatin and the Doré series to be Timiskaming in age. He concluded that the Doré series was compressed into east-west trending synclines, and anticlines which were later removed by erosion during Algoman time, and that the major faulting took place during Keweenawan time.

Tanton (1948) reported that the oldest rocks of the Helen Iron Range surround and include the Helen Iron Formation. South of the oldest rocks are altered sediments, greenstones, pyroclastics, and intrusive quartz porphyries. North of the oldest rocks occur massive and schistose greenstone intruded by a body of quartz porphyry. He recognized two members of iron formation: a siliceous ironstone member and a siderite member. Tanton thought the iron ore bodies were formed by the near complete replacement of the host rocks by ascending solutions of magmatic origin.

Goodwin (1960) described the Michipicoten rocks as an assortment of contemporaneous volcanic and sedimentary rocks surrounded by younger regional granites. He believed that the iron formations in the area were genetically related to the volcanic-sedimentary succession. Goodwin interpreted the area to be folded about east-west trending axes with a central anticline surrounded by flanking synclines that in turn were cross folded about north trending axes. He also reported that the district was broken into several large blocks by north-striking, vertical faults with large scale left-lateral displacements.

Goodwin (1962) stated that the Michipicoten rocks were the result of a subaqueous repeating volcanic cycle that was initiated by the eruption of mafic to intermediate flows followed by the rapid discharge of pyroclastic rocks. This was followed by hot spring and fumarolic activity that resulted in the deposition of the iron formations. He thought the iron, carbonate, and sulfur were of subvolcanic and/or magmatic origin and that the silica came from the leaching of the volcanic wall rocks by hot spring and fumarolic solutions.

Goodwin (1964) reported on the stratigraphy and the chemical zonation of the Helen Iron Range. He found that the iron range is zoned (lithologically) from rhyolites in the western portion to rhyodacites and dacites in the central portion to dacites in the eastern portion. He reported that the footwall volcanic complex was intensely altered up to 60 m below the iron formation. Stratigraphically below the intensely altered zone, a weak alteration zone several hundred meters thick, is imprinted on the footwall volcanic complex. Goodwin believed the alteration of the Helen Iron Range rocks took place shortly after their emplacement by the fumarolic and hotspring solutions that deposited the Helen Iron Formation.

The Ontario Geologic Survey has maintained mapping parties in the Michipicoten district for years, notable among them being Rupert's (1975) party which mapped (at one inch equals one quarter mile) McMurray Township and parts of adjacent townships. Currently the Ontario Geologic Survey has mapping crews under R. Sage working on or completing geologic maps of Chabanel, Esquega, Lastheels, and McMurray townships, District of Algoma.

Goodwin, et al., (1976) reported on recent research done on the origin of the Helen Iron Formation. They concluded that the Michipicoten iron formations developed by the subaqueous chemical precipitation of volcanically derived components. They believe the silica came from the leaching of the volcanic wall rocks and the sulfur was from the biologic reduction of seawater sulfate. Sulfur and carbon isotope data indicates the existence of autotropic organisms in the Archean Michipicoten basins and supports the proposed role of photosynthesis in the formation of the banded iron formations.

La Tour, et al., (1980) described the chloritoid-bearing hanging-wall pillow lavas of the Helen Iron Range and speculated as to the factors controlling the thermochemical stability of the chloritoid.

Algoma Exploration and the Algoma Steel Corporation have also maintained geologic crews in the area for many years. Their latest project (1979-1981) has been an exploration program for massive sulfides that resulted in both chemical analyses of select samples and the compilation of a regional geologic map of the Michipicoten district at one inch equals one half mile.

## I.5 Acknowledgements

The author wishes to thank Algoma Exploration Ltd. for permission to work on the property of the Algoma Steel Corporation and for financial support for this study.

The author also wishes to expressly thank Dr. Ronald L. Morton of the Geology Department of the University of Minnesota-Duluth without whose help and encouragement this project would not have been possible.

Thanks are also extended to Drs. John C. Green and Ralph W. Marsden for serving on the author's examining committee and to the staff and students of the University of Minnesota-Duluth Geology Department for many stimulating and enjoyable times in the last two years.

The author also wishes to thank his wife, Julie, for putting up with him during the course of his study at the University of Minnesota-Duluth.

## I.6 Regional Geology

The Michipicoten district is located in the Abitibi-Michipicoten greenstone belt in the Superior structural province of the Canadian shield. Sources of information on the regional geology of the district are taken from Rupert's (1975) map (P. 828 of the Ontario Geological Survey) which was used as a base map for Algoma Explorations' (1979-1981) massive sulfide project, and from Algoma Explorations' (1979-1981) map. Figure 2 (regional geology of the district) is a compilation from the above two sources plus the author's mapping.

Rupert (1975) shows that the Michipicoten area can be divided into several distinct geologic areas on the basis of dominant lithology, structural style, and metamorphic grade. The central part of the map area, south of Wawa Lake and west of the Walbank Lake fault, (Figure 2), is characterized by intermediate to felsic metavolcanics with minor occurrences of intermediate to felsic intrusive rocks. Structurally this central area is characterized by moderate to steep dips and by open fold styles. Metamorphic grade is middle greenschist facies.

In the second part of the area, north of Wawa Lake (Figure 2), the rocks are, in stratigraphic order, rhyolite lava and pyroclastic flows, iron formations, pillowed and massive basalts, and volcanogenic sedimentary rocks. Sills and/or dikes of carbonate-rich metagabbro intrude the rhyolites, iron formations and the lowermost basalts. Dips in this area are steep to overturned. Fold patterns are similar to cross-sections of recumbent nappe folds suggesting that small scale nappe folding and transport may have occurred prior to a period of isoclinal folding. The metamorphic grade is lower greenschist facies.

The third major division of the Michipicoten area, east of the Walbank Lake Fault and south of Wawa Lake, (Figure 2), is composed dominantly of basalts with interbedded felsic volcanic rocks and iron formation. Granitic dikes are relatively common throughout this part of the area and many can be traced back into granite intrusions exposed to the south of the area. Dips are moderate to steep. The metamorphic grade in the area ranges from greenschist in the north to amphibolite in the south (near the contacts with large granitic bodies).

The Archean rocks of the Michipicoten area are intruded by north-northwest and northeast-trending gabbroic dikes of Archean to Keweenawan ages. These dikes occupy regional fault zones that have significant horizontal and vertical movements.

The youngest rocks in the area are from the Firesand Carbonatite (Figure 2) dated by K-Ar methods at 1048 million years b.p. (Wanless, et al., 1969).

The last recessional ice front in the Michipicoten area was in contact with the waters of proglacial Lake Stanley-Houghton. Minong stage terraces at Wawa are located at 300 m and 120 m above Lake Superior. The valleys of the Magpie and Firesand rivers are Minong stage estuaries of Lake Superior (Rupert, 1975).

Figure 2

Regional Geology

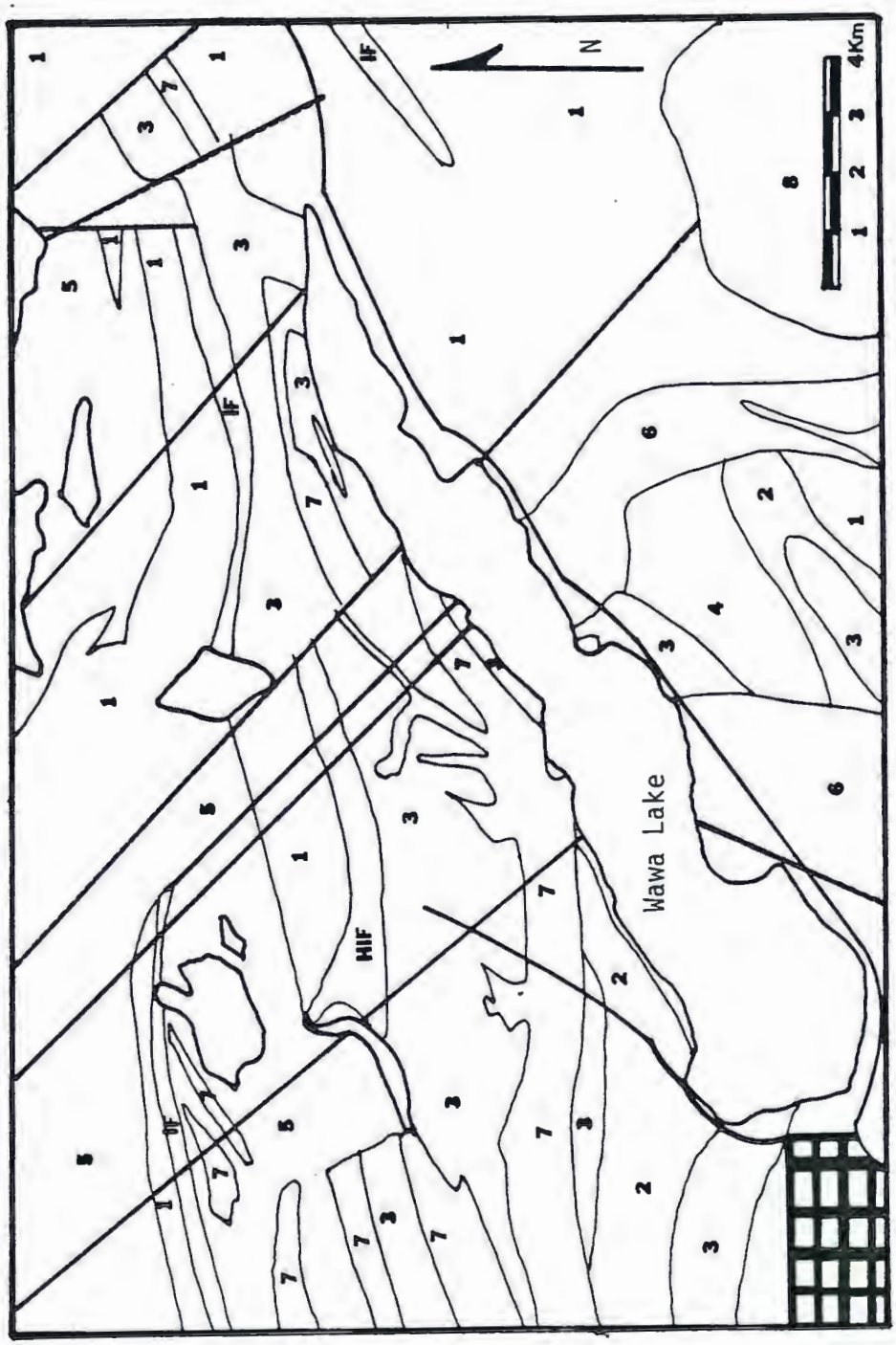

Figure 2

General Geology Map

Legend

| | |
|---|---|
| 8 | Firesand Carbonate. |
| 7 | Mafic and Ultramafic Rocks. |
| 6 | Intermediate to Felsic Intrusive Rocks. |
| 5 | Dore Metasediments and Eleanor Slates. |
| 4 | Metasediments. |
| HIF | Helen Iron Formation. |
| IF | Iron Formation. |
| 3 | Felsic Metavolcanics. |
| 2 | Intermediate Metavolcanics. |
| 1 | Mafic Metavolcanics. |

Scale: 1 cm equals approximately .4 km.

Fault

Geologic Contact

Road

Outline of Present Study Area

Sources of Information:
Rupert, 1975: --OGS Prel. Map p. 828
Algoma Explor.: Upub. Map 1/2 Mile Compilation

# II: LITHOLOGY AND STRATIGRAPHY

## II.1 Introduction

The distribution of lithologic units in the thesis area is shown on Figure 3 (in jacket). Exceptional preservation of primary features permits interpretation of the original volcanic character of the rocks. Compositions of representative specimens of the volcanic rock units have been determined by chemical analyses (Chapter 3). For the sake of brevity the prefix "meta" is not used in the remainder of this text.

The felsic volcanics within the map area are part of a general sequence of mafic volcanics to felsic volcanics to iron formation which is capped by more mafic volcanics that pass upward into volcaniclastic sedimentary rocks. The felsic pile below the Helen Iron Formation is also cyclic. The rhyolitic succession passes from subaqueous phreatomagmatic pyroclastic deposits into pyroclastic deposits formed by sustained eruption column collapse. This sequence is repeated, and capped and intruded by rhyolitic domes and/or lava flows with associated dome-collapse deposits. The entire rhyolitic succession is capped by the Helen Iron Formation.

The following section on lithology includes descriptions of each rock type, including its apparent stratigraphic thickness, typical textures, and mineralogy. Modes and textures of individual specimens representative of separate rock types are listed in tabular form in Appendix I. Descriptions of the rocks are followed by descriptions of the structure and metamorphism.

## II.2 Descriptions of Rock Units

### Unit 1 Dome and/or Lava Flow Rhyolites

Dome and/or lava flow rhyolites are buff to dark gray, very fine-grained, and are aphyric to porphyritic. They are exposed in the north, northeast and extreme south portions of the map area (Figure 3) and reach a maximum apparent stratigraphic thickness of 350 to 400 meters with strike lengths of up to 1000 meters. These rocks are composed of quartz (60%), plagioclase (15%) and orthoclase (5%) with accessory amounts of sericite, siderite, chloritoid, epidote, tourmaline, stilpnomelane, hematite, magnetite, and pyrite (Appendix I, Table 1). On the basis of preserved primary textures these rocks may be divided into three distinct types: 1) massive, 2) flow laminated, and 3) spherulitic.

Massive Rhyolites Massive rhyolites are exposed in the northeast section of the map area (Figure 3) and are generally massive in appearance yet locally they may contain up to five percent, by volume, ash and lapilli size fragments. The fragments are all similar mineralogically to the matrix and are defined by a slightly coarser grain size than that of the matrix material. Fractured and broken quartz and feldspar phenocrysts, less than one mm in diameter, compose up to five percent of some samples. Phenocrysts and fragments are set in a fine-grained matrix of xenomophic, recrystallized quartz and plagioclase (Appendix I, Table 1). The feldspar is partly replaced by tiny disseminated sericite shreds. The rock is cut by numerous discontinuous stringers (.1-.5 mm wide) of sericite, chlorite, stilpnomelane, chloritoid, epidote, hematite, pyrite and siderite.

Flow-Laminated Rhyolites Flow-laminated rhyolites are similar mineralogically and texturally to massive rhyolites. The major difference is the presence of thin (1-10 mm wide) subparallel, contorted and convoluted flow laminae which are best seen in outcrop or hand specimen (Plate 1). The laminae, in thin section, are defined by and separated from each other by slightly coarser-grained, discontinuous veinlets of quartz and feldspar up to several cm long and half a mm wide. These tiny veinlets are also cut at oblique angles by other, similar-sized quartz veinlets.

Flow-laminated rhyolites are exposed in the north and northeast sections of the map area (Figure 3).

Spherulitic Rhyolites Spherulitic rhyolites are comprised of from ten to sixty percent spherulites which are separated from each other by a flow-laminated matrix (Plate 2). Individual spherulites are up to two cm in diameter, subround to oval in cross section, and are, for the most part, concentrically zoned. An inner zone which makes up one third to one half the diameter of the spherulite, is composed of a very fine grained (.1-.2 mm), interlocking mosaic of recrystallized quartz and feldspar that may or may not contain disseminated sericite shreds. The middle zone (one third to one quarter of the total diameter) is also a fine-grained mosaic of quartz and feldspar which exhibits outlines of grains approximately two times coarser (.4-.8 mm wide) than are now present (Plate 3). The outer zone (one third to one quarter total diameter) is much the same as the middle zone except the outlines of the larger grains are not present. In any given spherulite, one or more of the zones may be missing.

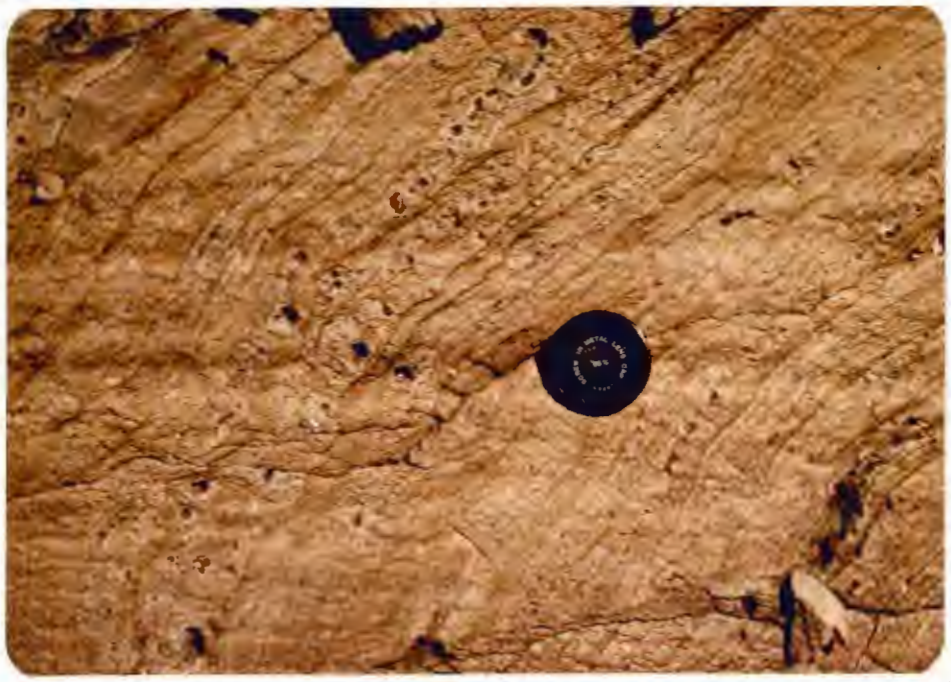

Plate 1: Flow Laminated Rhyolite with Lithophysae. (Scale is 55 mm in diameter.)

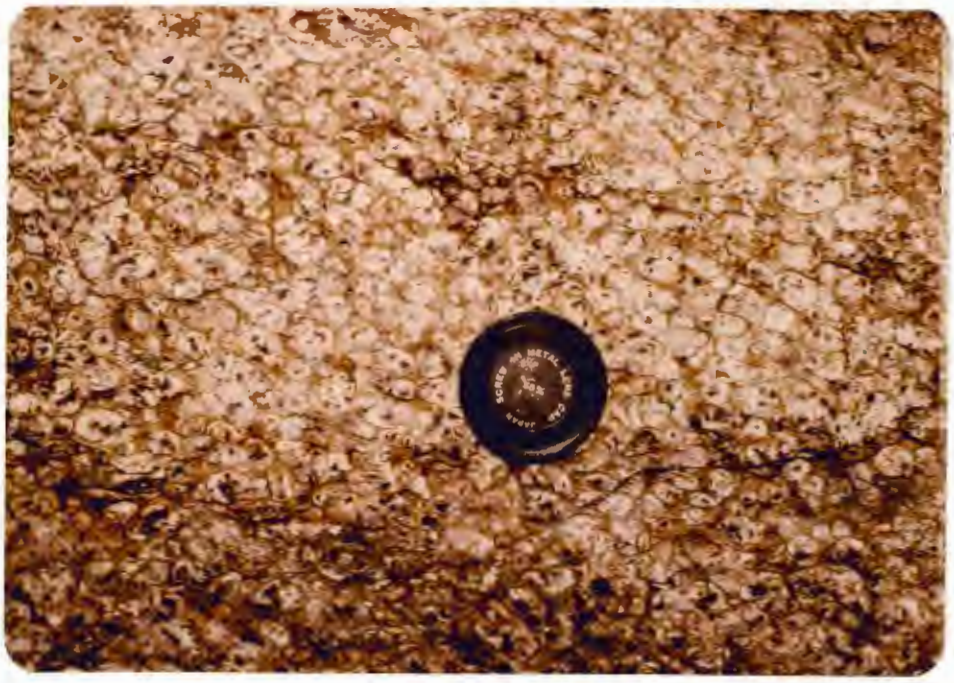

Plate 2: Spherulitic Rhyolite. (Scale is 55 mm in diameter.)

On the basis of the observed primary textures, these rocks are interpreted to represent portions of lava domes and/or lava flows.

Modes and textures of representative samples of dome and/or lava flow rhyolites are listed on Table 1, Appendix I.

Unit 2 Block, Lapilli, and Ash Pyroclastic Breccias

Coarse, poorly sorted, chaotic, rhyolitic, pyroclastic breccias are found in the north and northeast sections of the map area (Figure 3). They range in apparent stratigraphic thickness from 100 to 350 meters and occupy strike lengths of 200 to 700 meters.

The breccias are composed of cream to light brown, angular fragments that range in size from coarse ash to blocks a meter or more in diameter. Fragments make up from ten to sixty percent of the rock and are set in a fine grained (.2-.4 mm) matrix, often slightly finer grained and darker than the fragments themselves (Plate 4).

Fragments are of four main types: 1) massive, 2) flow laminated, 3) spherulitic, and 4) dense and vesiculated (juvenile). Type 4 is considered to be juvenile, that is, formed directly from the erupting magma, whereas fragment types 1, 2, and 3 have textural and mineralogical characteristics much like those seen in the dome and/or lava flow rhyolites and are considered accessory in origin (that is, they were fragments of solid rocks ripped off by the erupting magma). These first three fragment types compose from ten to forty percent of the rock and range in size from ash to blocks. Many of the block size fragments contain two to three mm wide milky quartz veins that are terminated at the fragment edges.

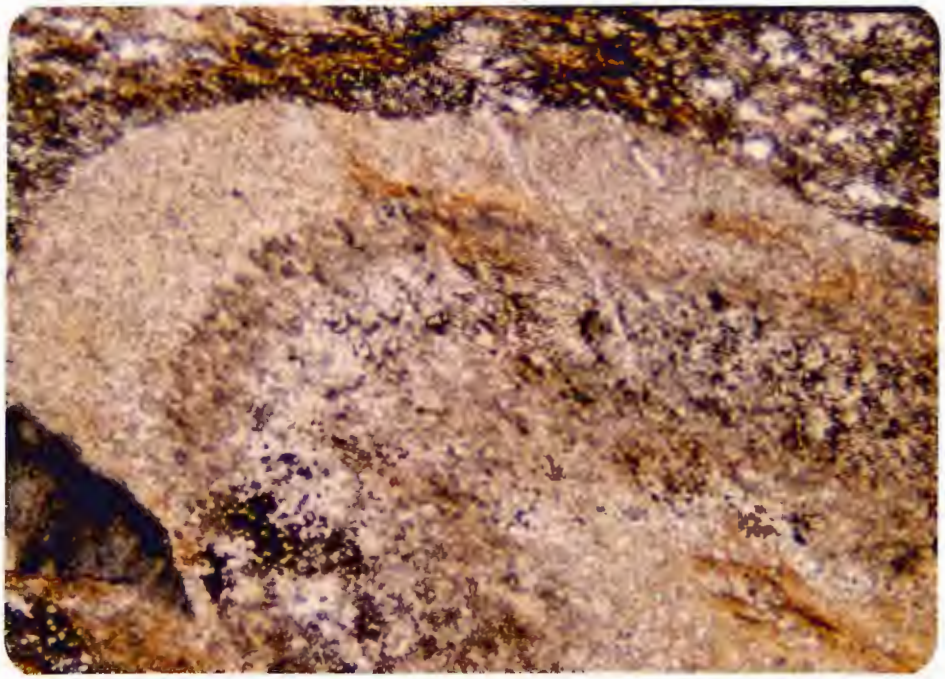

Plate 3: Photomicrograph of the zones of a spherulite. (Field of view 6 mm.)

Plate 4: Block and Ash Pyroclastic Breccia.

Juvenile fragments rarely exceed ten percent of the rock and are rarely larger than ash and lapilli. These fragments, in hand sample and outcrop, are dark brown (color index two to three times that of the matrix), angular, cuspate, elongate, or digitated clasts from one to two cm wide and from two to seven cm long (Plate 5). In thin section these fragments were observed to be composed of mosaics of fine-grained (.1-.2 mm diameter) quartz, plagioclase, and sericite with various associated opaque minerals (pyrite, hematite, magnetite, siderite, ilmenite, leucoxene). Individual juvenile clasts may be divided into three types based on mineralogical composition. Type a, (Plate 6), is composed of clear quartz and feldspar mosaics with minor disseminated sericite and opaques. Type b, (Plate 7), is composed almost entirely of sericite shreds with minor interstitial quartz and feldspar. Type c, (Plate 8), is composed almost entirely of very fine grained iron stained silicates with minor interstitial quartz, feldspar, and sericite. Plate 8 also shows tiny, internal, tubular structures interpreted as being long tube pumice. Fiske (1969, p. 3) concluded that long tube pumice is more typical of subaqueous deposits because pumice of this type has sufficient permeability to become waterlogged quickly and settle to the sea floor fairly close to its source area. Plate 8 also shows inter-fragment clear patches of quartz (.1-.2 mm wide) interpreted to be original uncollapsed vesicles or amygdules.

The matrix material is a fine grained (.1-.2 mm) interlocking mosaic composed dominantly of recrystallized quartz (50-80%) and feldspar (25-50%) with pervasive disseminated sericite and local areas of disseminated chlorite. Small stringers (.5-1 mm wide by 2-3 cm long) of sericite,

Plate 5: Pumice in outcrop. Pumices are dark, cospate shapes embedded lighter colored matrix. (Scale is 55 mm in diameter.)

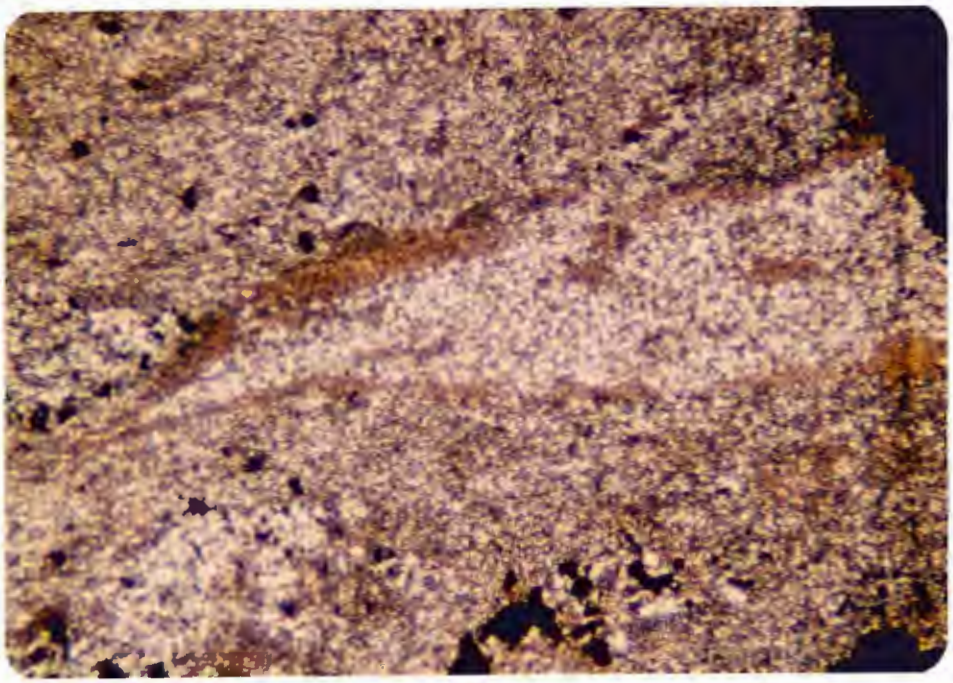

Plate 6: Photomicrograph showing type "a" pumice embedded in a recrystallized matrix composed of quartz and feldspar. Field of view is 5 mm across.

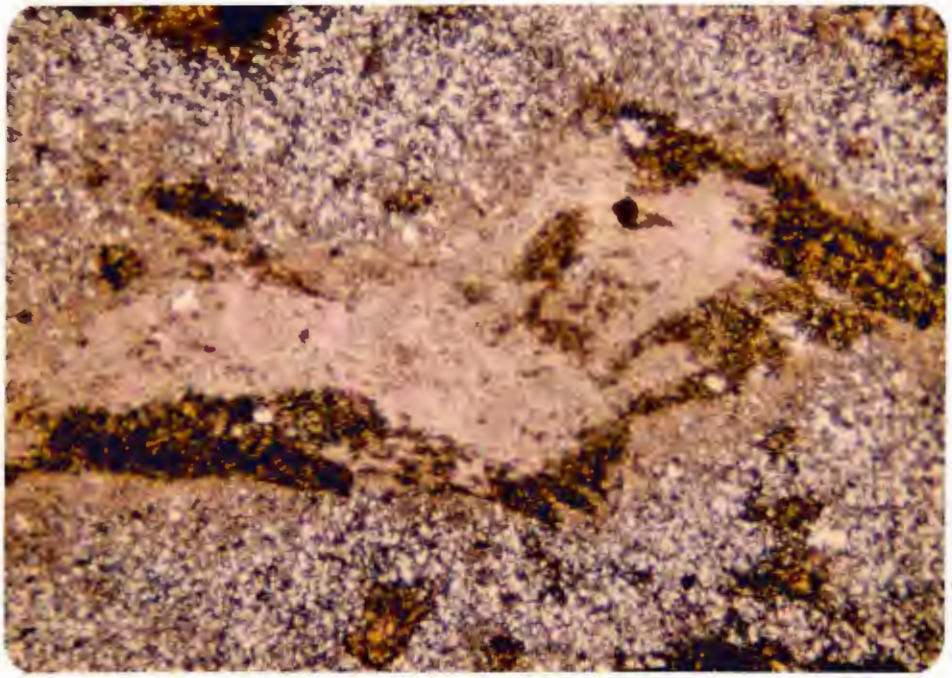

Plate 7: Photomicrograph of type "b" pumice embedded in quartz and feldspar matrix. Field of view is 6 mm.

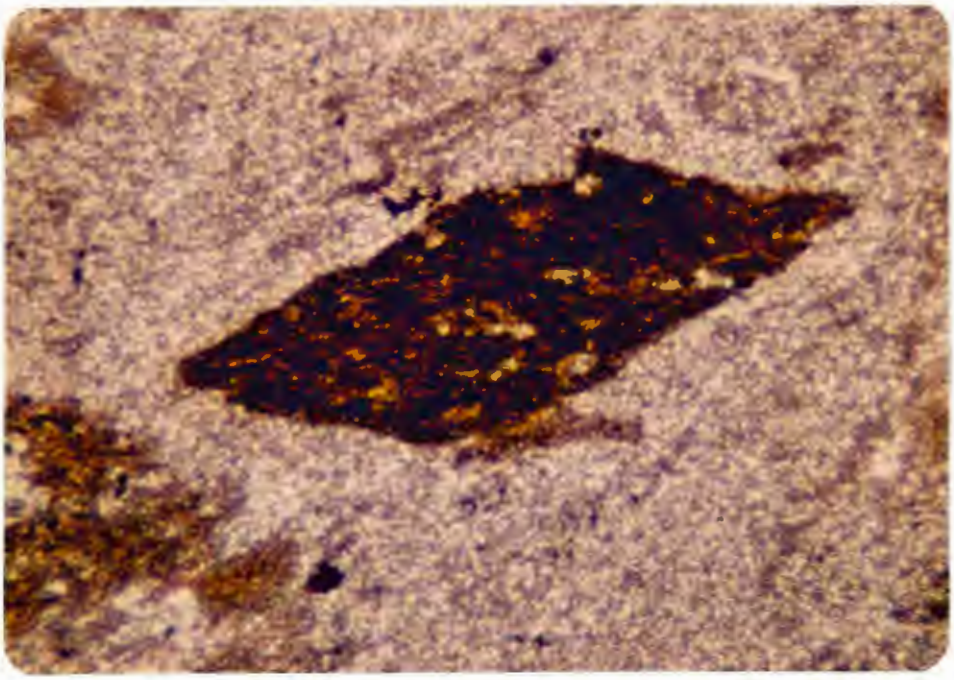

Plate 8: Photomicrograph of type "c" pumice embedded in quartz and feldspar matrix. Field of view is 4 mm.

chlorite, stilpnomelane, siderite, hematite, magnetite, pyrite, chloritoid, and epidote occur in minor amounts throughout the rock (Table 1, Appendix I).

Block and Ash Pyroclastic Breccias This breccia type is composed of from forty to sixty percent, by volume, block to coarse ash size fragments. Accessory fragment types make up from forty to fifty percent, by volume, with juvenile types composing the remainder. These block and ash pyroclastic deposits grade outward into lapilli and ash tuff breccias.

Lapilli Tuffs This unit is composed of from ten to forty percent, by volume, lapilli and ash size fragments. (Accessory/juvenile clast ratios are similar to block and ash breccias.)

These breccia deposits are believed to represent pyroclastic block and ash, and lapilli and ash flows that originated by sloughing off of the sides of growing domes and/or lava flows. This conclusion is based on the following: 1) accessory fragment types which are very similar to the dome and/or lava flow rhyolites, 2) the presence of up to ten percent lapilli to ash size juvenile fragments, 3) the extremely poor sorting of the breccias and 4) their proximity to the dome and/or lava flow rhyolites. The block and ash flows appear to represent a near source facies with the lapilli and ash flows representing a more distal facies.

Unit 3 Massive Pyroclastic Flow Rhyolites

Massive pyroclastic flow rhyolites range from quartz and feldspar porphyries lacking visible fragmental texture to vesiculated aphyric juvenile lapilli tuffs and tuffs. These rocks make up forty to fifty

percent of the felsic succession in the map area (Figure 3) and may reach 350 to 400 meters in apparent stratigraphic thickness with strike lengths of at least 1000 meters.

Crystal Tuffs Crystal tuffs are located in areas southwest of Moran Lake and east of Algoma Steel's sinter plant (Figure 3). They range in apparent stratigraphic thickness from 300 to 400 meters and are exposed for distances of more than 1000 meters.

The crystal tuffs are cream to dark brown rocks which contain from ten to thirty percent fine (.5-1 mm) to medium grained (1-3 mm), fractured, broken, and/or partially resorbed quartz and plagioclase phenocrysts. The phenocrysts are set in a fine grained matrix (.1-.5 mm) composed primarily of quartz (40-60%), plagioclase (10-30%) and orthoclase (10-15%) with accessory amounts of sericite, carbonate, chlorite, stilpnomelane, siderite, hematite, pyrite, magnetite, ilmenite, and leucoxene (Table 1, Appendix I). Up to ten percent block to ash size accessory and juvenile lithic fragments are also embedded in the matrix material, which is probably devitrified and recrystallized vitric ash.

In both hand sample and outcrop the crystal tuffs show little lithic variation (Plate 9). They lack primary lamination or bedding features by which they can be further divided, but on the basis of phenocryst mineralogy, as determined in thin section, they may be subdivided into two separate groups.


Plate 9: Crystal Tuff. Scale is 55 mm in diameter.

Plagioclase-phyric Tuffs The bulk of the crystal tuffs contain both plagioclase and quartz phenocrysts; their plagioclase/quartz phenocryst ratios range from 3.5 to 0.75 and are here called plagioclase-phyric tuffs. Plagioclase is mostly medium grained (1-3 mm) and moderately to intensely altered to sericite and carbonate. Quartz is mostly fine grained (.5-1 mm) and unaltered. Rarely the rock may contain one to five percent fine grained (.5-1 mm) potassium feldspar phenocrysts.

The anorthite content of the plagioclase phenocrysts was determined by optical methods (Michel-Levy and/or Carlsbad-Albite twin methods) where the plagioclase was well enough preserved to permit extinction angle determinations, and from cation norms (Baragar and Irvine, 1971) calculated from whole rock chemical analyses (Appendix II, Table 2). The plagioclase, as determined by these methods, with few exceptions was albite ($An_3$-$An_7$). The exceptions gave (Baragar and Irvine) normative andesine.

Quartz-phyric Tuffs The second group of crystal tuffs contains dominantly quartz phenocrysts (Appendix I, Table 1). They have plagioclase/quartz phenocryst ratios less than 0.5 and are gradational into plagioclase-phyric tuffs southwest of Moran Lake. There is thus a distinct mineralogical zonation from plagioclase-rich to quartz-rich tuffs with increasing stratigraphic height (tops to north). These rocks range in apparent stratigraphic thickness from 75 to 150 meters.

Pumice-Bearing, Rhyolitic Lapilli Tuffs Pumice-bearing lapilli and ash deposits overlie the crystal tuffs and are exposed in the areas west of Moran Lake and east of Algoma Steel's sinter plant (Figure 3).

The rock ranges in color from gray to light brown and typically contains from one to five percent fine grained (.5-1 mm) quartz phenocrysts. Pumice fragments are ash to lapilli and compose from twenty-five to forty-five percent, by volume, of the rock (Plate 10; detailed descriptions of pumice in outcrop and thin section are given in chapter II.2).

Accessory fragments are composed of flow laminated and/or massive rhyolite, similar to the dome and/or lava flow rhyolites.

The matrix material is similar mineralogically and texturally to the matrix material of the crystal tuffs (Table 1, Appendix I).

On the basis of the presence of unwelded crystal tuff sequences topped stratigraphically by unwelded pumice-bearing tuffs, massive pyroclastic flow rhyolites are interpreted to have been deposited either as quenched subaqueous pyroclastic flows derived from the continuous collapse of a sustained, partially subaqueous, partially subaerial eruption column, or from pyroclastic flows derived from the continuous column collapse of a subaerial eruption column.

Unit 4 Laminated Rhyolitic Tuffs Laminated rhyolitic tuffs occur in the south half of the map area (Figure 3). Laminated tuffs rarely reach more than fifty meters in apparent stratigraphic thickness and range along strike from 100 to 300 meters. These rocks are light gray to pale brown and very fine grained. In outcrop, individual laminae vary from a few mm to five to ten cm thick, being roughly the same order of magnitude in thickness at any one locality. The laminae vary from gently crossbedded and convoluted to plane parallel (Plate 11).

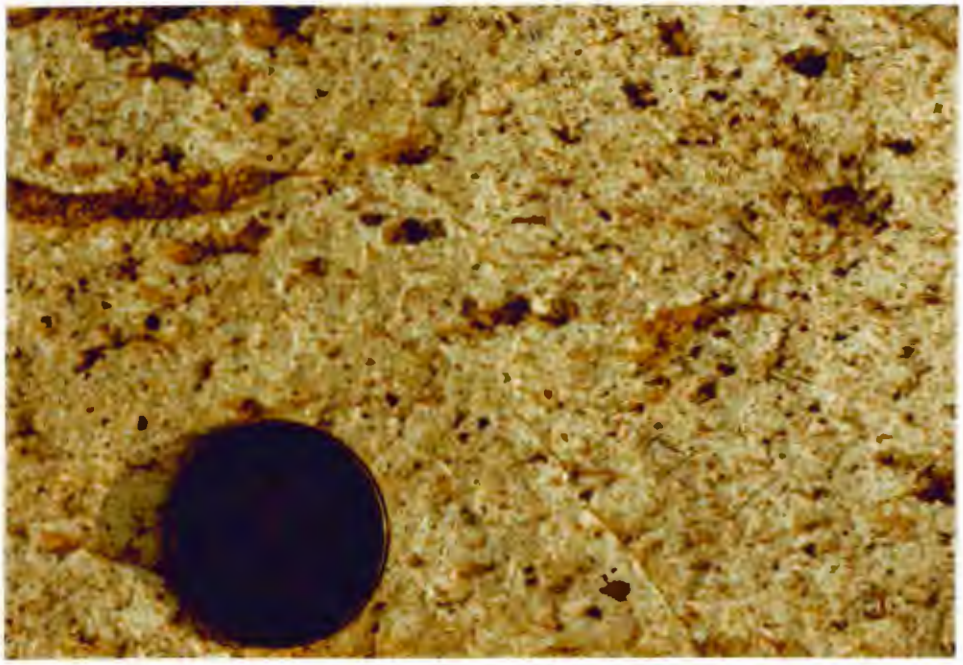

Plate 10: Pumice-bearing Tuff. (Scale is 55 mm in diameter.)

Plate 11: Laminated Hyalotuffs. (Scale is 55 mm in diameter.)

Some zones contain up to twenty percent fine grained (.5-1 mm) fractured, broken, and/or partially resorbed phenocrysts, mainly of quartz with five to twenty-five percent of the phenocrysts composed of plagioclase. They also contain from one to five percent ash to lapilli size pumice fragments.

The finely bedded zones locally contain up to forty percent, fine to medium grained, concentrically zoned spheroids in the lapilli and ash size range. Petrographically, three types of spheroidal lapilli were observed, often occurring together. Crystal cored spheroids were observed with rims of aphanitic, optically continuous material surrounding partially resorbed quartz phenocrysts (Plate 12). Similar features in thin sections from Keweenawan lava flows were shown to the author by Dr. John C. Green (1981, personal communication) that are interpreted to be devitrification overgrowths on phenocrysts. An alternative interpretation is that these spheroids are accretionary lapilli. The second type of spheroid observed are zoned mosaics of quartz and feldspar (Plate 13). The show coarse grained cores (ten times coarser grain size than rim layers) up to two-thirds the diameter of the particle of quartz and feldspar surrounded by one or more very fine grained rim layers (one-third diameter of particle). The coarse grained center may be a rock fragment, possibly a type "a" pumice fragment. This particle type of spheroid is believed to be an armored accretionary lapilli. R. L. Morton (1981, personal communication) states "armored accretionary lapilli are a variety of accretionary lapilli that contain crystal or rock fragment nuclei coated by a thin rind of fine ash and have only been reported from hydroclastic deposits." The last type of spheroid are zoned, aphanitic

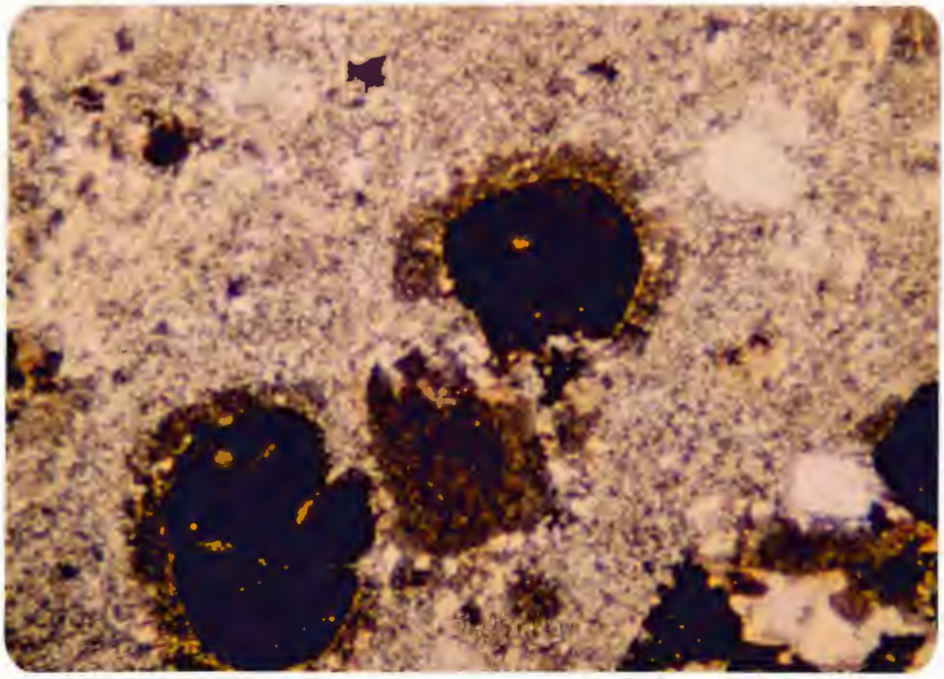

Plate 12: Photomicrograph of crystal cored spheroid showing devitrification rims. The fragments could also possibly be armored accretionary lapilli. Field of view is 4 mm.

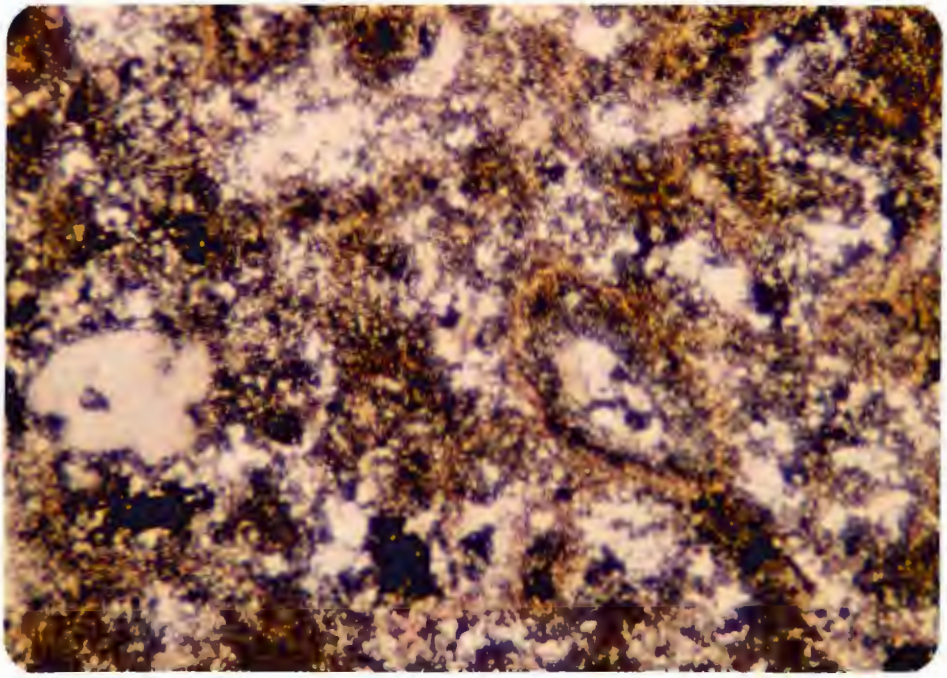

Plate 13: Photomicrograph of rock-cored accretionary lapillus. Field of view 4 mm.

mosaics of quartz and feldspar. They show cores (up to two-thirds the diameter of the particle) of radiating aggregates of quartz and feldspar (Plate 14). The outer rim is made up of fine grained (.05 mm) material. It is not uncommon to see two or more cores stuck together and then covered by a rim layer (Plate 14). This type of spheroid probably has a similar origin to the first type of spheroid discussed (e.g., post-depositional "diagenetic" features). However, they may also be clotted accretionary lapilli. R. L. Morton (1981, personal communication) states that clotted accretionary lapilli have only been observed in phreatomagmatic deposits.

Laminated rhyolitic tuffs are similar mineralogically to the other felsic rocks described (Table 1, Appendix I). The presence of the fine grained, gently crossbedded, contorted, convoluted, and/or plane parallel beds associated with possible accretionary lapilli suggest that these rocks are hyalotuffs formed from subaqueous phreatomagmatic eruptions. The hyalotuffs overlie bedded pyroclastic flow deposits and are thought to represent the ash-rich portion of an upward fining sequence of the type described by Fiske and Matsuda, (1964).

Unit 5 Bedded Rhyolitic Lapilli Tuffs

Bedded lapilli tuffs are exposed in the southeast and south corners of the map area (Figure 3). These rocks reach a maximum apparent stratigraphic thickness of fifty to seventy meters and strike lengths of 100 to 300 meters. They are light gray to pale brown and contain from twenty to forty percent ash to lapilli-size clasts composed of massive and flow-laminated lithic fragments (30-35%) and pumiceous and dense juvenile

fragments (0-10%) set in a fine grained matrix. Individual beds vary from five to fifteen cm thick and exhibit a crude (normal) grading of lithic clasts, coarser clasts towards south of any bed. Occasional block and bomb size fragments are also present. An exposure showing an aerodynamically shaped bomb with symmetrical bomb-sag bedding features is located approximately 100 meters north-northwest of the Ontario Ministry of Natural Resources Building on the northeast outskirts of Wawa (Plate 15). Symmetrical bomb-sag bedding features are believed by R. V. Fisher (1980) to be suggestive of subaqueous environments of deposition.

These rocks are similar mineralogically to the felsic volcanic rocks previously described (Table 1, Appendix I). The bedding, sorting, fragment composition, and associated symmetrical bomb-sagged beds, suggest that these rocks are subaqueous pyroclastic flow deposits derived from the initial stages of phreatomagmatic eruptions that produced the hyalotuffs. These bedded pyroclastic flow deposits are thought to represent the dense fragment portion of an upward fining sequence of the type described by Fiske and Matsuda, (1964).

Unit 6 Dacites and Andesites

Dacites and/or andesites are exposed in the area directly southwest of Moran Lake and in the southern half of the map area (Figure 3). They reach maximum apparent stratigraphic thickness of approximately 600 meters and strike lengths of 1000 to 1400 meters. These rocks comprise fifteen to twenty percent of the volcanic succession. This group of rocks ranges from dacite to andesite according to whole rock chemical analyses,

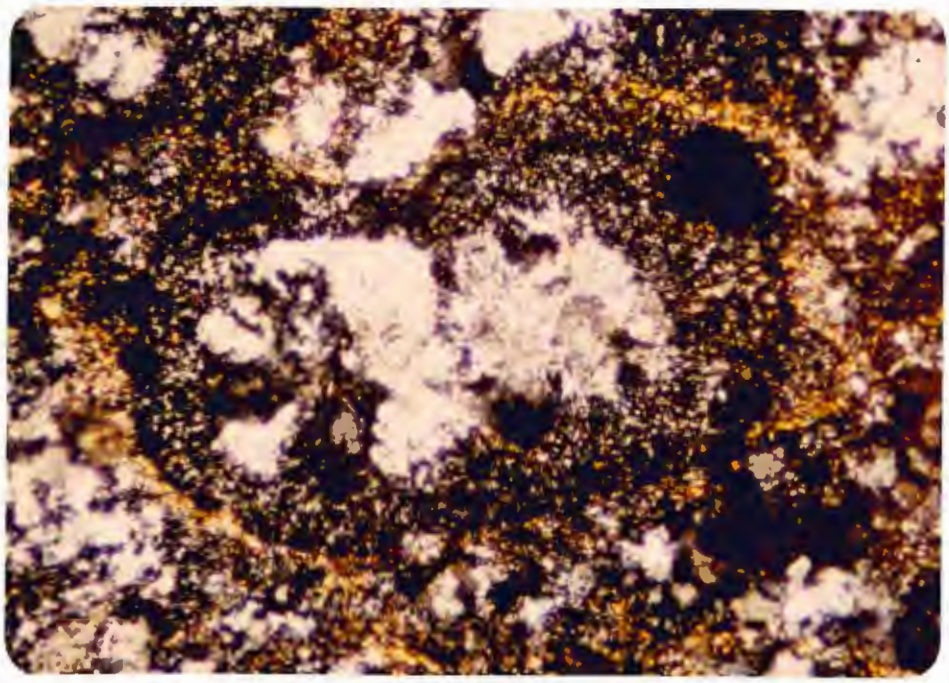

Plate 14: Photomicrograph of clotted spheroid embedded in matrix of quartz and feldspar. Possibly could be a clotted accretionary lapillus. Field of view 4 mm.

Plate 15: Bedded, pyroclastic flow deposit with bomb and bomb-sagged bed features.

relict diabasic textures, and secondary mineral assemblages (Table 1, Appendix I) and will be referred to here as andesite.

In outcrops the andesites are chlorite-rich and gray to dark brown. On the basis of preserved primary textures they are divided into four lithological types: 1) massive lava flows or subvolcanic intrusions, 2) coarse, matrix-supported pillow breccias, 3) pyroclastic flow deposits and 4) massive, intensely altered, lava flow deposits.

Andesite Massive Lava Flows (or Subvolcanic Intrusions) These rocks are exposed in the area southwest of Moran Lake. They reach maximum apparent stratigraphic thickness of twenty to thirty meters and strike lengths of up to 100 meters.

The andesite lava flows or subvolcanic intrusions are massive and very fine grained. In thin section they exhibit relict poikilitic textures with up to thirty percent medium to coarse grained (3-6 mm), subround to oval clots of recrystallized quartz and feldspar which are interpreted as relict amygdules (Plate 16). Mineralogically these rocks contain quartz (20%), plagioclase (50%), chlorite (10%), and carbonate (10%) with minor and varying amounts of sericite, stilpnomelane, tourmaline, biotite, siderite, and various opaque minerals (ilmenite, leucoxene, pyrite) (Table 1, Appendix I).

On the basis of preserved diabasic textures and amygdules, these rocks are interpreted to be subvolcanic intrusions and/or lava flows.

Andesite Pillow Breccias Andesite matrix-supported breccias are exposed southwest of Moran Lake (Figure 3). They reach a maximum apparent stratigraphic thickness of twenty to thirty meters and strike lengths of 300 to 400 meters.

These rocks contain twenty to thirty percent, angular to subround, poorly sorted, block-size fragments set in a dark, igneous matrix (Plate 17). The blocky, subround fragments surrounded by rims at different material suggest possible pillow shapes. The fragments and matrix, in thin section, are aphanitic, aphyric, xenomorphic mosaics of recrystallized quartz (10%) and plagioclase (10%) with intense secondary alteration of sericite (20%) and chlorite (50%) (Table 1, Appendix I). Where less altered, a relict diabasic texture may be seen in both the fragments and the matrix, relating them to the andesite lava flows.

The pillow shaped fragments set in an igneous matrix suggest these rocks to be pillow breccia deposits.

Andesite Pyroclastic Breccias Andesitic pyroclastic breccias crop out southwest of Moran Lake and in the south part of the map area (Figure 3). They comprise fifty to seventy percent of the dacite-andesite succession and range from 100 to 250 meters in thickness with lengths along strike of up to 1000 meters.

These rocks contain from twenty to fifty percent angular, unsorted fragments, ranging in size from blocks to ash (Plate 18), set in a very fine-grained (.1-.2 mm) matrix. The fragments are dominantly massive and accessory in origin (15-45%). Minor amounts of pumice (0-5%) and rare quartz (1%) and plagioclase (1%) phenocrysts (.5-2 mm) are also present. At a few localities the fragments are preferentially orientated with their long axes trending approximately $80^{o}$, which parallels regional bedding.

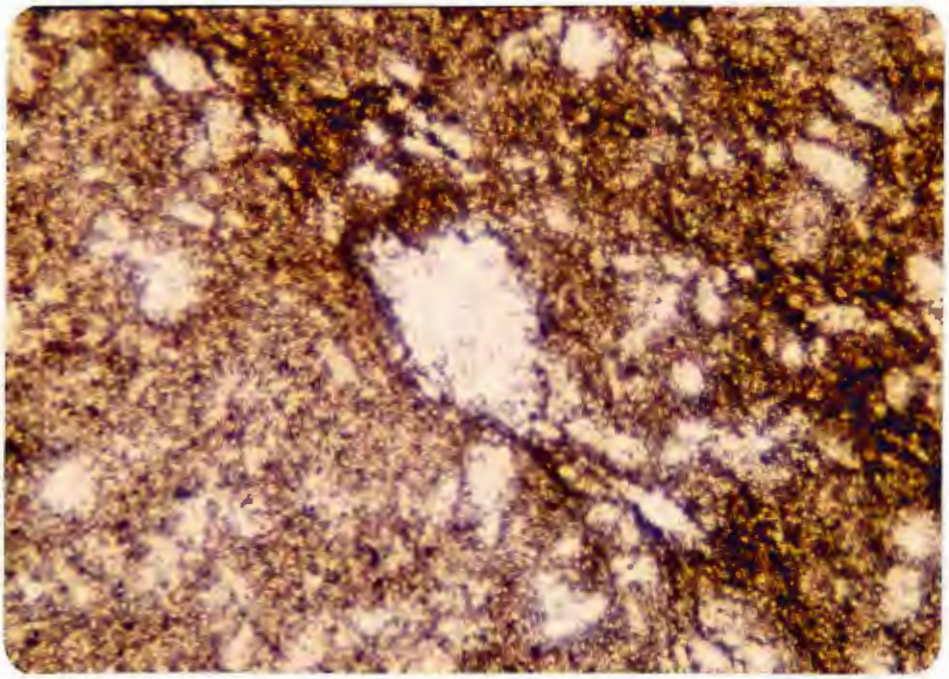

Plate 16: Photomicrograph of dacite-andesite subvolcanic intrusion and/or lava flow. It shows relict plagioclase laths set in an aphanitic matrix of chlorite and carbonate. Relict amygdule is outlined. Field of view is 4 mm.

Plate 17: Andesite Pillow Breccia. Scale is 55 mm in diameter.

Mineralogically the fragments are composed of recrystallized mosaics of quartz (20%), plagioclase (30%), sericite (5-10%), chlorite (15-30%), and carbonate (10-20%) with varying minor amounts of pyrite, hematite, siderite, ilmenite, leucoxene, and magnetite (Table 1, Appendix I). Locally, accessory lithic fragments exhibit a relict diabasic texture.

Matrix material for these rocks is composed of quartz (20-30%), plagioclase (30-40%), and chlorite (10-30%) with variable, but minor, amounts of sericite, carbonate siderite, and various opaque minerals (pyrite, ilmenite, leucoxene, hematite, magnetite) (Table 1, Appendix I).

On the basis of preserved primary textures and the nature of the fragment types, these rocks are thought to represent pyroclastic flow deposits associated with vents that produced the andesite lava flows (and/or subvolcanic intrusions) and the andesite pillow breccias.

Massive, Intensely Altered Lava Flow Andesites These rocks crop out in the south half of the map area (Figure 3) and comprise from thirty to fifty percent of the andesite succession. The best outcrops are located on road cuts along the Helen mine road in the south half of the map area.

These andesites are gray, aphanitic, and massive. In thin section they are very fine-grained (.1 mm), xenomorphic mosaics of recrystallized plagioclase (10-25%), quartz (5-10%), carbonate (30-40%), and chlorite (20-30%) with variable amounts of pyrite, siderite, hematite, magnetite, ilmenite, and leucoxene (Table 1, Appendix I).

These rocks probably are intensely altered massive lava flows that may have been related to the vents that produced the other andesites. This interpretation is suggested by the lack of any recognizable primary texture and on the basis of similar mineralogical associations with other andesites.

Unit IF Helen Iron Formation

The Helen Iron Formation has been extensively studied and described by other workers so only a brief description will be given here.

The Helen Iron Formation at the Helen Mine consists of an upper banded chert member (60-250 m thick) (Plate 19), a middle massive pyrite member (2-20 m thick), and a lower massive siderite member (maximum 110 m thick) which extends along strike for more than 3000 meters.

The iron formation is underlain comformably and gradationally by the previously described felsic dome and/or lava flow and associated Merapi type pyroclastic flow deposits, and overlain with sharp contacts by mafic pillowed volcanic rocks.

Unit 7 Gabbroic Dikes

The last igneous event in the map area was the emplacement of easterly, northwest-southeast and northeast-southwest trending gabbroic dikes. Four ages of these dikes are recognized.

Quartz-Bearing Gabbro The oldest mafic body forms a W shaped intrusion to the east of Moran Lake (Figure 3). This intrusive body is a medium-grained, hypidiomorphic rock made up of carbonate (ankerite, 60%) and chlorite (25%) with minor amounts of quartz (8%) and

Plate 18: Andesite pyroclastic breccia. Scale is 55 mm in diameter.

Plate 19: Banded chert member of the Helen Iron Formation. The scale is 55 mm in diameter.

plagioclase (7%). This rock is highly altered, yet local areas show poikilitic textures suggesting relict ophitic growth and a gabbroic lithology. This intrusive body is cut by northwest-trending dikes of the following rock type.

Quartz-Bearing Pyroxene-Hornblende Gabbro These dikes are fine to medium-grained, hypidiomorphic, ophitic rocks composed of plagioclase ($An_{44}$, 40%) and moderately to intensely altered pyroxene (augite?, 40%) with minor quartz (5%) and amphibole (5%). Slickensides show that these dikes are sites of later faulting. A rock with a similar composition also forms the large east-trending intrusion (dike or sill) in the southern half of the map area. Here the dike varies from fine-grained at the edges to coarse-grained at the center.

Quartz-Bearing Pyroxene-Hornblende Gabbro Quartz-bearing pyroxene-hornblende gabbro dikes cut both of the previously described dikes. These rocks are medium-grained and hypidiomorphic. In hand sample they appear very similar to the quartz-bearing pyroxene-hornblende gabbro, however, in thin section, they are unaltered. They are composed chiefly of labradorite ($An_{60}$, 45%) and augite (45%) with minor amounts of quartz (5%) and hornblende (5%).

Quartz-Bearing Biotite-Pyroxene Diabase The last intrusive rock type to be described within the map area is reddish-brown, very fine-grained (.1-.2 mm), and amygdaloidal with ten percent medium to coarse grained (3-6 mm in diameter) amygdules in a hypidiomorphic groundmass which exhibits a diabasic texture. This rock is composed of slightly

to moderately altered plagioclase (50%), biotite (20%), and pyroxene (augite?, 20%) with minor amounts of quartz (5%) and sericite (5%). This dike cuts the felsic volcanics, yet is not observed to cut any other dikes.

## II.3 Alteration

One of the main objectives of this study was to describe the post-volcanic changes that have taken place within the felsic volcanics of the Helen Iron Range footwall (Chapter 1.1). This section will describe the alteration of the footwall volcanic rocks; Chapter III.3 identifies the mobile constituents involved in the alteration.

Incipient silicification and sericitization are ubiquitous throughout the area (Chapter II, III). Goodwin (1964) also described the Helen Iron Range footwall rocks as being altered. He described an intense alteration zone for a distance of sixty meters beneath the iron formation and a less intense alteration zone for another 700 to 1000 meters. Recent work by Algoma Exploration has outlined an alteration "pipe" extending below the Helen Iron Formation for a distance of approximately 1000 meters. The main alteration pipe (Figure 3) is defined by porphyroblasts (1-5 mm across) of chloritoid which may be accompanied by variable amounts of chlorite, epidote, and carbonate along with ubiquitous quartz and sericite. Near the iron formation, in the intensely altered zone, the matrix of the wall rock is replaced by fine-grained, dark reddish-brown siderite (Plate 20) and various opaque minerals (hematite, magnetite, pyrite).

In this study, using petrographic and outcrop analyses, a number of separate episodes of veining are recognized. The earliest veining episode is represented by quartz veins observed in outcrops of felsic block, lapilli, and ash pyroclastic breccias. This veining occurred prior to brecciation as the veins extend through fragments and are truncated at the fragment-matrix boundary. This period of vein formation must be early and not related to the episodes which produced the alteration pipe. A second episode, seen in the same felsic block, lapilli, and ash pyroclastic breccias and in the dome and/or lava flow rhyolites, produced quartz-siderite-magnetite veins that cut both matrix and fragments of felsic volcanic rocks as seen in thin section. The third episode, seen in thin section in the same rocks as the second vein episode occurs in, produced sericite and/or chlorite, chloritoid, epidote, and stilpnomelane stringers and veinlets. The fouth episode, seen in thin section in similar rocks as the second and third episodes, produced quartz veinlets and stringers without any opaques.

## II.4 Stratigraphy

The felsic volcanic rocks of the Helen Iron Range footwall are cyclic in eruptive history. The rhyolite succession passes from subaqueous phreatomagmatic pyroclastic deposits into pyroclastic flow deposits produced from sustained collapse of an eruption column. This sequence is then repeated, and capped and intruded by rhyolite dome and/or lava flows with associated dome collapse deposits and iron formation (Chapter II.1). Figure 4 is a generalized stratigraphic column for the map area, illustrating the cyclic nature of the felsic volcanism which occurred in the area.

Figure 4

Generalized Stratigraphy of Study Area

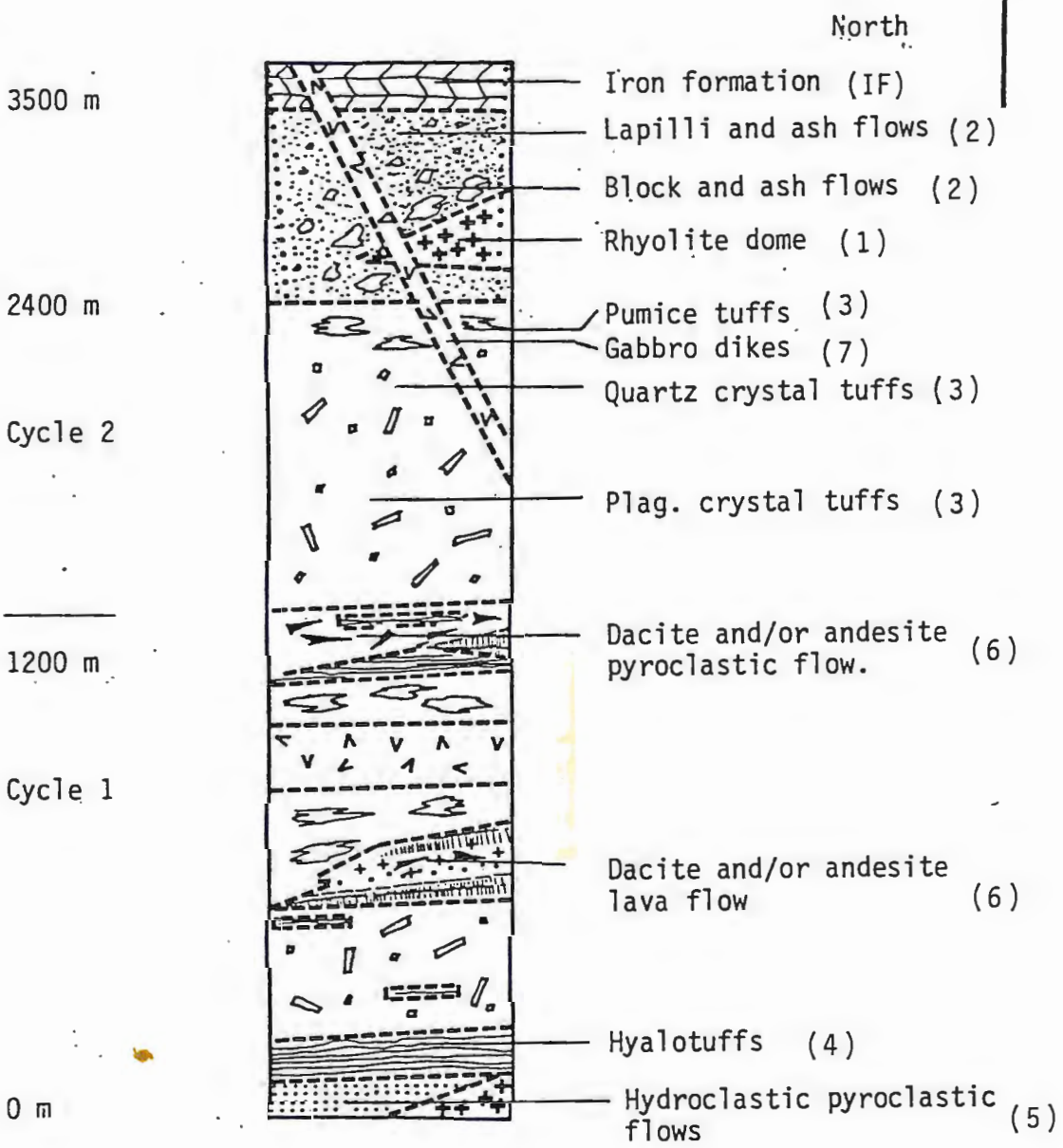

Figure 4 Legend

| | |
|---|---|
| Gabbro Dikes. | (Unit 7) |
| Helen Iron Formation. | (Unit IF) |
| Block and Ash Flows. | (Unit 2) |
| Lapilli and Ash Flows. | (Unit 2) |
| Rhyolite Dome. | (Unit 1) |
| Pumice Tuffs. | (Unit 3) |
| Quartz Crystal Tuffs. | (Unit 3) |
| Plag. Crystal Tuffs. | (Unit 3) |
| (Dacite-)Andesite Pyroclastic Flow. | (Unit 6) |
| (Dacite-)Andesite Lava Flow. | (Unit 6) |
| Massive (Dacite-)Andesite. | (Unit 6) |
| Hyalotuff. | (Unit 4) |
| Hydroclastic Pyroclastic Flow Deposits. | (Unit 5) |

Plate 20: Intense alteration zone below the Helen Iron Formation where the matrix of lapilli and ash tuff breccia was replaced by siderite and various opaque minerals (hematite, magnetite, pyrite). Scale is 55 mm in diameter.

The first volcanic cycle began with subaqueous phreatomagmatic eruptions in the form of bedded, rhyolitic pyroclastic flow deposits (Unit 5) and hyalotuffs (Unit 4). The uppermost hyalotuff unit is overlain by crystal tuffs (Unit 3) that, in turn, grade into pumice-bearing lapilli and ash pyroclastic flow deposits (Unit 3). Interbedded with the pumice-bearing tuffs are andesitic pyroclastic and/or lava flows (Unit 6) that are believed to have originated from a vent that was not related to the source vent for the rhyolites. The top of the interbedded pumice-bearing tuff, andesite sequence is thought to represent the end of the first cycle of volcanism.

The second volcanic cycle consists of another series of bedded pyroclastic flows and hyalotuffs that are interbedded with andesitic pyroclastic flows, lava flows, and intrusive breccia deposits. Stratigraphically overlying the andesites occurs another crystal tuff sequence that is zoned with a bottom rich in plagioclase crystals and a top rich in quartz crystals. A pumice-bearing tuff sequence caps the crystal tuffs. Towards the end of this second cycle of subaqueous (subaerial?) volcanism, rhyolite domes and/or lava flows (Unit 1) with associated Merapi-type pyroclastic flow deposits (Unit 2) were emplaced above the crystal tuffs, pumice-bearing tuffs, hyalotuffs, and bedded pyroclastic flow deposits. Block-and-ash flow deposits occur proximal to the domes and lapilli-and-ash flow deposits are distal to the domes.

The last phase of felsic volcanism in the area was the fumarolic and hot spring activity that resulted in the development of an alteration pipe and the deposition of the Helen Iron Formation. The last igneous activity seen in this part of the Helen Iron Range was the emplacement of the various gabbroic dikes (Unit 7).

## II.5 Structure of the Map Area

The structure of the Michipicoten area has been variously described as being crossfolded anticline-syncline pairs (Goodwin, 1962) and, in the area of the Helen Iron Range, as being similar to cross sections of recumbent nappe folds (Rupert, 1975). Suffice it to say, the structure of the region is probably very complex and it is beyond the scope and the objectives of this study to attempt to delineate regional structural styles.

Within the map area, bedding in the rocks generally trends east-northeast and dips moderately to steeply south while topping to the north, making the whole succession slightly overturned. Good top indicators are found in the bomb-sagged and normally-graded beds in the southeast and southwest portions of the map area, in the succession felsic volcanics-Helen Iron Formation-mafic pillowed volcanics in the north of the area, and in the presence of the alteration pipe in the Helen footwall volcanics.

Faults have been inferred where significant airphoto lineaments indicate their possible presence. Two major faults are interpreted to be present in the map area. The northwest-southeast and northeast-southwest trending quartz-bearing pyroxene-hornblende gabbro dikes observed in the north section of the map area are slickensided and are thought to be localized along fault zones. The valley that runs from the southwest corner of Moran Lake to the sinter plant is a pronounced lineament that could be a major fault zone. Many small lineaments were observed that may be sites of minor fault activity.

## II.6 Metamorphism of the Study Area

One of the main reasons for selecting the footwall rocks of the Helen Iron Range for this study is the low degree of metamorphism and of penetrative deformation the rocks have undergone. Many outcrops show well-preserved primary textures and structures allowing interpretation of their original volcanic character. The rocks are recrystallized on a microscopic scale into interlocking mosaics of quartz and feldspar, yet primary petrographic textures are remarkably well preserved. The regional metamorphism in the map area is lower greenschist facies (Rupert, 1975) characterized by chlorite, epidote, biotite, stilpnomelane, and carbonate. This is superimposed on the earlier higher-temperature alteration associated with the footwall pipe.

# III: PETROCHEMISTRY

## III.1 Introduction

Classification of rocks in the thesis area is based primarily on field and petrographic criteria; however, the compositions of the various rock types were substantiated by chemical analyses of representative specimens. Chemical analyses and cation norms (Irvine and Baragar, 1971) of the volcanic and plutonic rock types are presented in tabular form in Appendix II.

## III.2 Sampling and Analyses

The locations of specimens selected for chemical analyses are shown as solid squares on Figure 3. The number beside each square corresponds with the number of the analysis presented in Appendix II.

Twenty-five samples were analyzed for ten major and twelve minor elements by Technical Service Laboratories, Mississauga, Ontario, using Inductively Coupled Argon Plasma (ICAP) methods. The author also had available data from an additional seven whole-rock chemical analyses completed on samples collected within or near the limits of the study area by Algoma Exploration.

## III.3 Correction for Metasomatism

The analyses reported in Table 1, Appendix II represent the raw chemical data which is uncorrected for metasomatic change. Also tabulated in Appendix II (Table 2) are adjusted values which have been corrected for detectable metasomatic changes by the method of Beswick and Soucie (1978).

Beswick and Soucie (1978) described a graphical procedure by which analytical data for a suite of metavolcanic rocks may be tested for, and within experimental limits, corrected for metasomatic modification of original compositions. The authors plotted the analytical data from 543 post-Mesozoic volcanic rock samples on Log Molecular Proportion Ratio (LMPR) plots. This data produces well defined trends that are taken as limits within which non-metasomatized samples should fall.

On any particular LMPR plot (e.g., log X/Z vs. log Y/Z) X metasomatism will displace the original composition parallel to the X/Z axis, Y metasomatism will displace the original composition parallel to the Y/Z axis, and Z metasomatism will displace the original composition along a line with a $45^{o}$ slope (Beswick and Soucie, 1978, p. 239).

The method assumes; firstly, that the metavolcanic suite to be corrected had initial compositions that would fit within the well defined trends on the various LMPR plots; secondly, that $Al_2O_3$ remains immobile during metasomatism; and thirdly, that $SiO_2$ remains relatively immobile during metasomatism.

Seven LMPR plots were used in Beswick and Soucie's (1978) original study to give an internally consistent set of numbers for the oxides $SiO_2$, $Al_2O_3$, $K_2O$, Fm (FeO + MgO), CaO, and $Na_2O$. It is not possible to determine the individual changes in the compositions of FeO and MgO, here collectively treated as Fm, without knowledge of the original FeO/MgO value of the rock. Figures 5a-5g show the LMPR plots on which a single sample (number 22, Appendix II) has been plotted to demonstrate the correction procedure.

Within the present study area, no zones of intense silicification were identified, although incipient silicification is ubiquitous, satisfying Beswick and Soucie's (1978) third requirement. In addition, the analyzed samples exhibit good to exceptionally well-preserved primary textures. This strongly indicates that the rocks have undergone no substantial volume changes and thus eliminates the need for mass balance calculations.

In figure 5a the demonstration sample (sample 22, Appendix II) is plotted in terms of its analyzed $SiO_2/K_2O$ and $Al_2O_3/K_2$ values and is designated point x; the limits of the trends for modern suites are also shown. In order to satisfy the requirements stated above and to move the analysis within the trend limits of the modern suites, a decrease in original value of $SiO_2$ to point a' (68% $SiO_2$) and an accompanying decrease in $K_2O$ (2.75%) to point a is necessary.

Figure 5b shows the same sample and the trend lines for modern suites on a $CaO/K_2O$ vs. $Al_2O_3/K_2O$ LMPR plot. Corrected values of $K_2O$ and $Al_2O_3$ are plotted with the uncorrected value of CaO. An increase of 4.19% CaO is necessary to bring the sample within the modern trend limits.

Figure 5

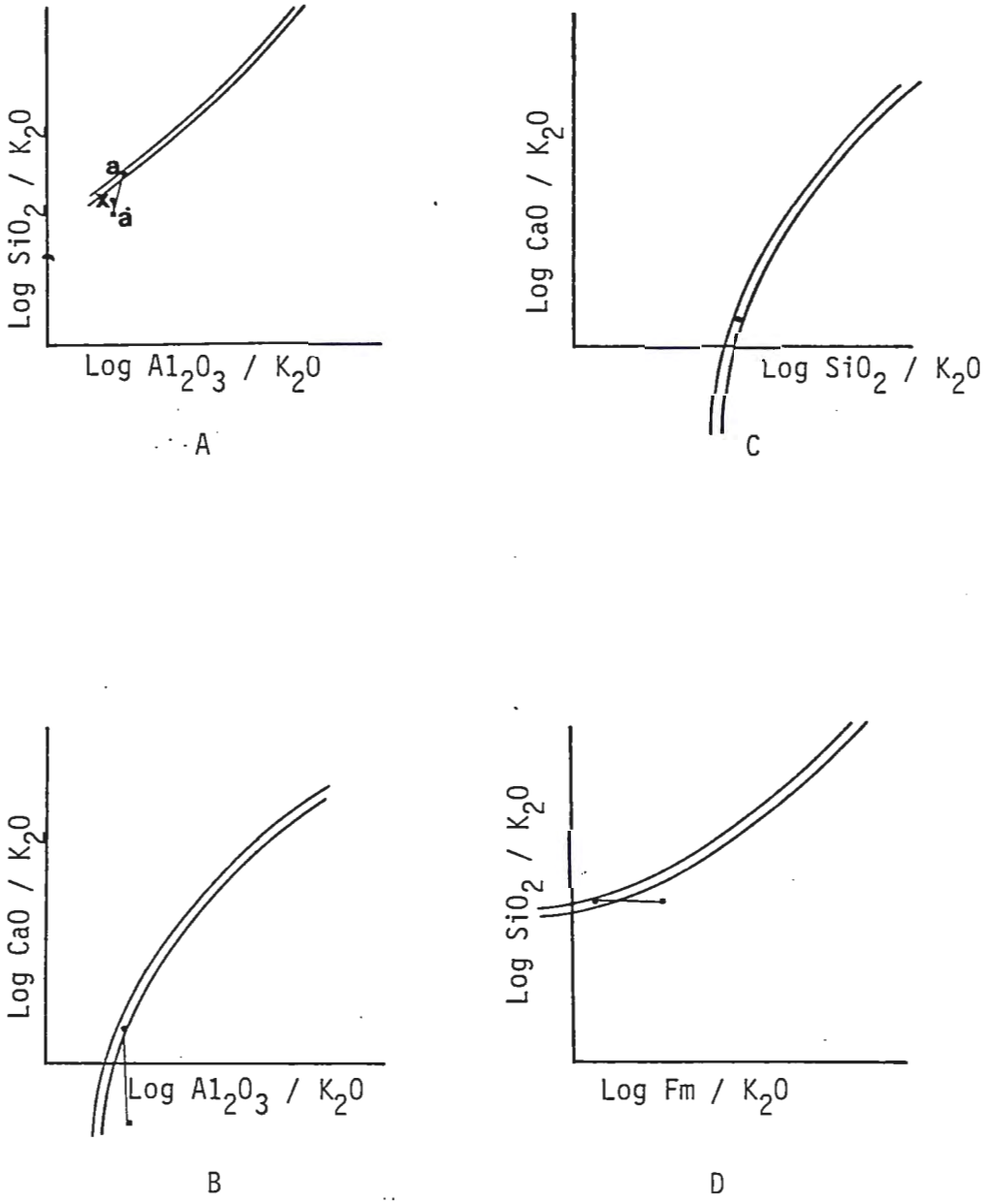


Log Molecular Proportion Ratio Plots

Figure 5

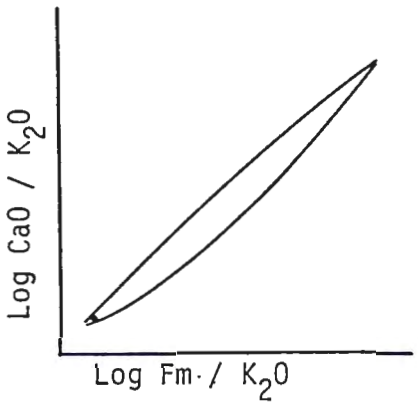
Log CaO / $K_2O$
Log Fm / $K_2O$

E

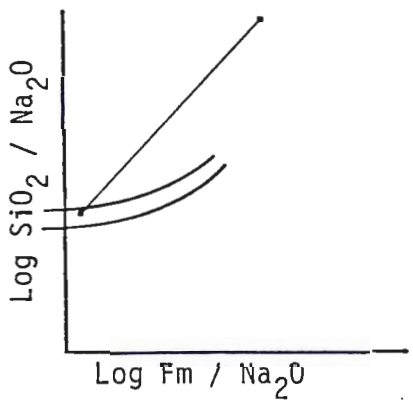
Log $SiO_2$ / $Na_2O$
Log Fm / $Na_2O$

F

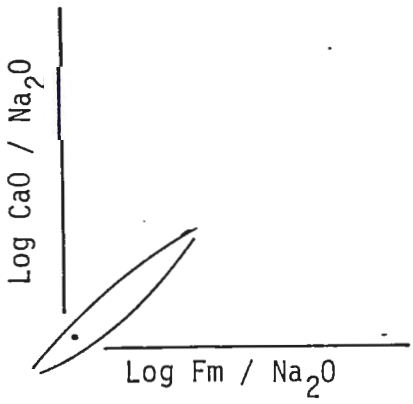
Log CaO / $Na_2O$
Log Fm / $Na_2O$

G

Figure 5c shows the same sample on a $CaO/K_2O$ vs. $SiO_2/K_2O$ LMPR plot using the above $SiO_2$, $K_2O$, and CaO corrections. It can be seen that the analysis plots within the modern trend lines. In Figure 5d the sample is shown on a $SiO_2/K_2O$ vs. $Fm/K_2O$ LMPR plot ($SiO_2$, $K_2O$ previously corrected values) with Fm having to be increased to 4.25% in order to bring the sample within the modern limits. In Figure 5e the sample is plotted on $CaO/K_2O$ vs. $Fm/K_2O$ LMPR plot using already corrected values. The sample plots within the modern trend lines requiring no additional modification of CaO, $K_2O$, or Fm. In Figure 5f, the sample is plotted on a $SiO_2/Na_2O$ vs. $Fm/Na_2O$ LMPR plot using corrected values of $SiO_2$ and Fm and uncorrected value of $Na_2O$. Here an increase in $Na_2O$ to 4.0% is needed to bring the analysis within the trend lines. Lastly the sample is plotted on Figure 5g, a $CaO/Na_2O$ vs. $Fm/Na_2O$ LMPR plot using previously corrected values. The sample plots within the trend lines for the modern suites requiring no further modification to be made to $Na_2O$, CaO, or Fm values.

The corrected and uncorrected values for sample 22 are listed on Table III.1. Both corrected and uncorrected values for the analyses are listed in Appendix II.

Table III.1

| | $SiO_2$ | $Al_2O_3$ | Fm | CaO | $Na_2O$ | $K_2O$ | LOI |
|---|---|---|---|---|---|---|---|
| Uncorrected | 74.41 | 14.47 | 2.14 | 0.81 | 0.10 | 4.13 | 1.76 |
| Corrected | 68.0 | 14.47 | 4.25 | 5.0 | 4.0 | 2.75 | - |
| Gain or Loss due to Metasomatism | gain | equal | loss | loss | loss | gain | |

Beswick and Soucie (1978) state that since the method to correct for metasomatic modification requires the assumption of constant $Al_2O_3$ and minimal $SiO_2$ change the values derived from the procedure are not absolute. The method is useful, however, in determining the relative gains and losses the samples have undergone during metasomatism. Table 3, Appendix II shows the relative gains and losses suffered by samples from the study area. Within the thesis area, $SiO_2$ has been added; Fm, CaO, and $Na_2O$ depleted, and $K_2O$ in about one half the cases depleted, and one half the cases added. In this regard, it is interesting to note that the Helen Iron Formation that sits above the metasomatized felsic volcanic units is high in Fe and Ca (Goodwin, 1964) constituents lost from the felsic volcanic rocks.

## III.4 Classification

As an additional check on the (Beswick and Soucie, 1978) correction procedure for metasomatism, the analyses were plotted on an alkali ratio plot (Hughes, 1972). Figure 6 (after Hughes, 1972) shows the plotted positions of both corrected and uncorrected analyses. Twenty-two of the thirty-two uncorrected values fall outside the field of the igneous spectrum in which all normal igneous rocks should fall (Hughes, 1972). The correction procedure described in Section III.3 moves all twenty-two of the metasomatized samples back into the field of the igneous spectrum. Through the use of the Hughes (1972) igneous spectrum (Figure 6) and Beswick and Soucie's (1978) metasomatism correction procedure, classification of whole rock analyses on standard petrochemical diagrams is considered more valid than if metasomatism was ignored.

Figure 6

Alkali Igneous Spectrum

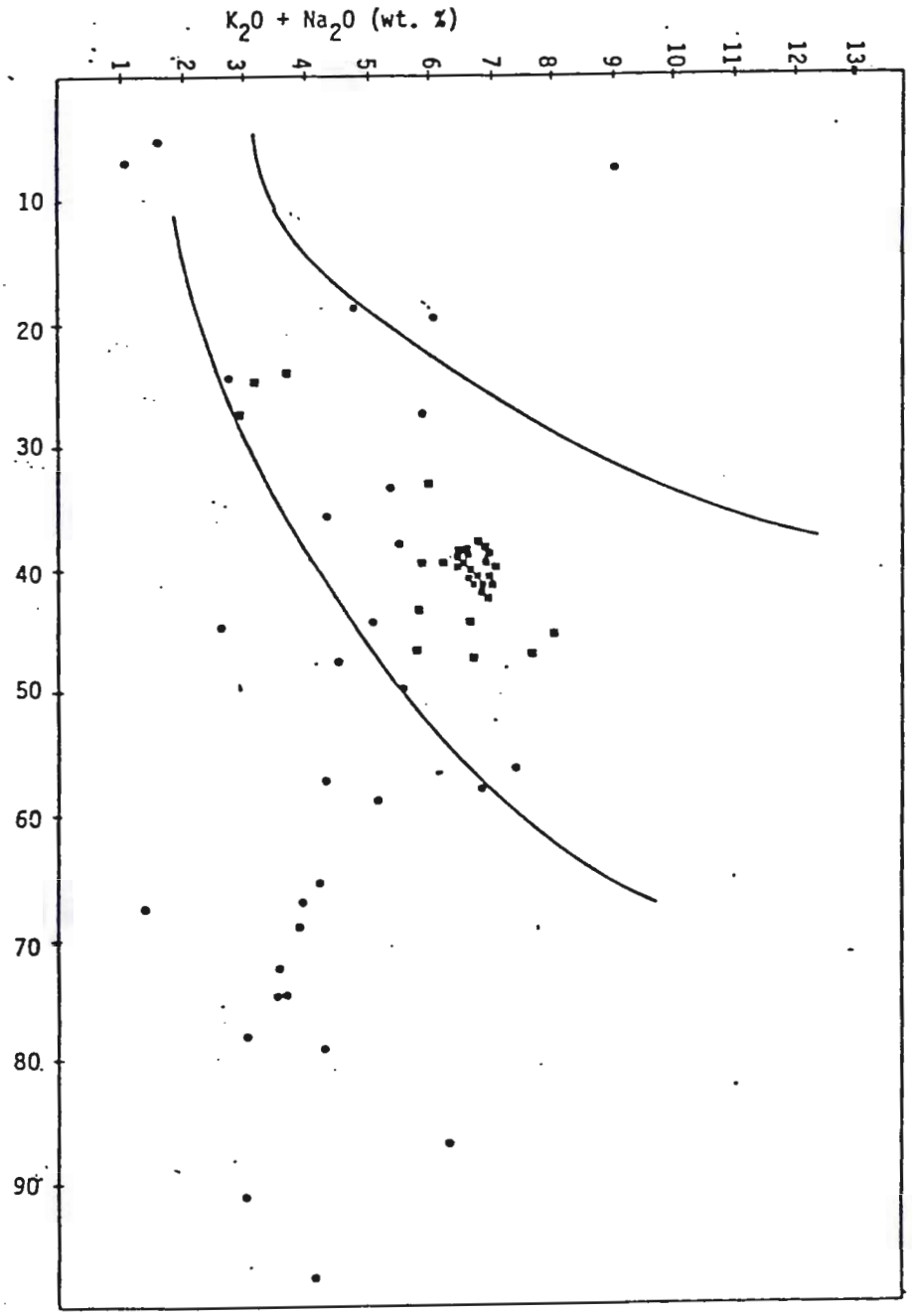

One of the main criteria used in selecting petrochemical diagrams for use in this study was the requirement that FeO and MgO could not be distinguished from each other since FeO and MgO were collectively referred to as Fm in the metasomatism correction procedure (see Section III.3). Therefore, diagrams such as the AFM diagram were not used.

Irvine and Baragar, (1971) used an alkalis vs. $SiO_2$ plot (Figure 7) to differentiate alkaline from subalkaline suites. Both uncorrected and corrected values of samples from the study area plot within the subalkaline field. The differentiation of subalkaline suites into tholeiitic or calc-alkaline was not possible as no mafic volcanic rocks are associated with the felsic volcanic rocks within the thesis area.

Taylor (1969) used a $K_2O$ vs. $SiO_2$ plot to differentiate calc-alkalic from tholeiitic suites; he also subdivided the plot into rhyolite, dacite, andesite, and basalt fields (Figure 8). Analyses which have not been corrected for metasomatism plot in both the calc-alkalic and tholeiitic fields (normal rhyolite and dacite); however, all samples fall into the calc-alkalic field after metasomatism correction. Four analyses of mafic dikes that cut the felsic rocks plot in the andesite, low K andesite, and low K basaltic-andesite fields.

## III.5 Minor Elements

Trace element analyses were undertaken with the aim of confirming field and petrographic interpretations as well as to delineate possible zonation within the pyroclastic flow units.

Figure 7

Alkali $SiO_2$ Diagram of Volcanic Rocks and Intrusive Rocks of the Helen Iron Range

(after Irvine and Baragar, 1972)

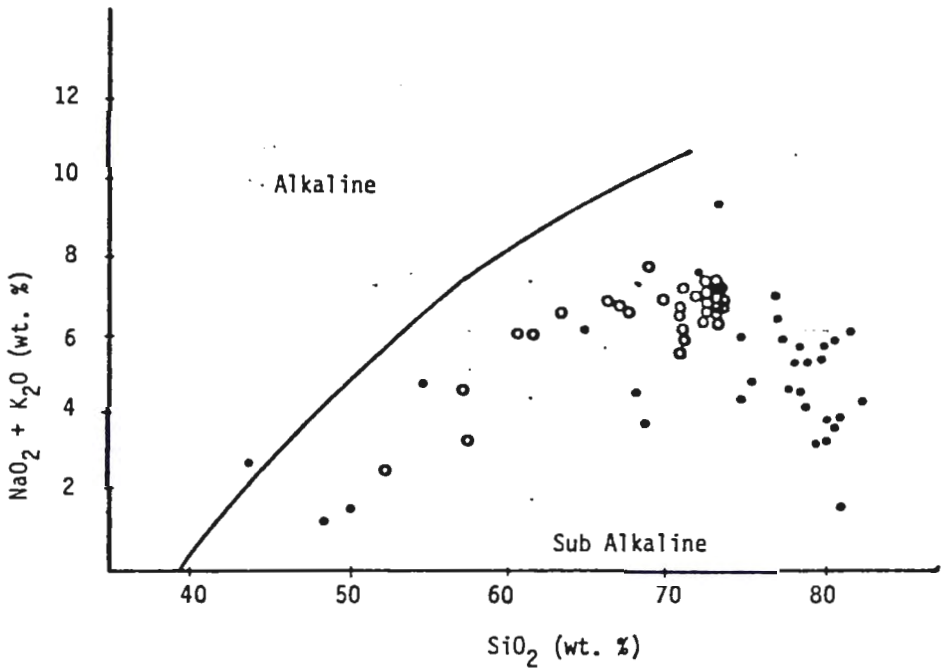


• uncorrected values

o corrected values

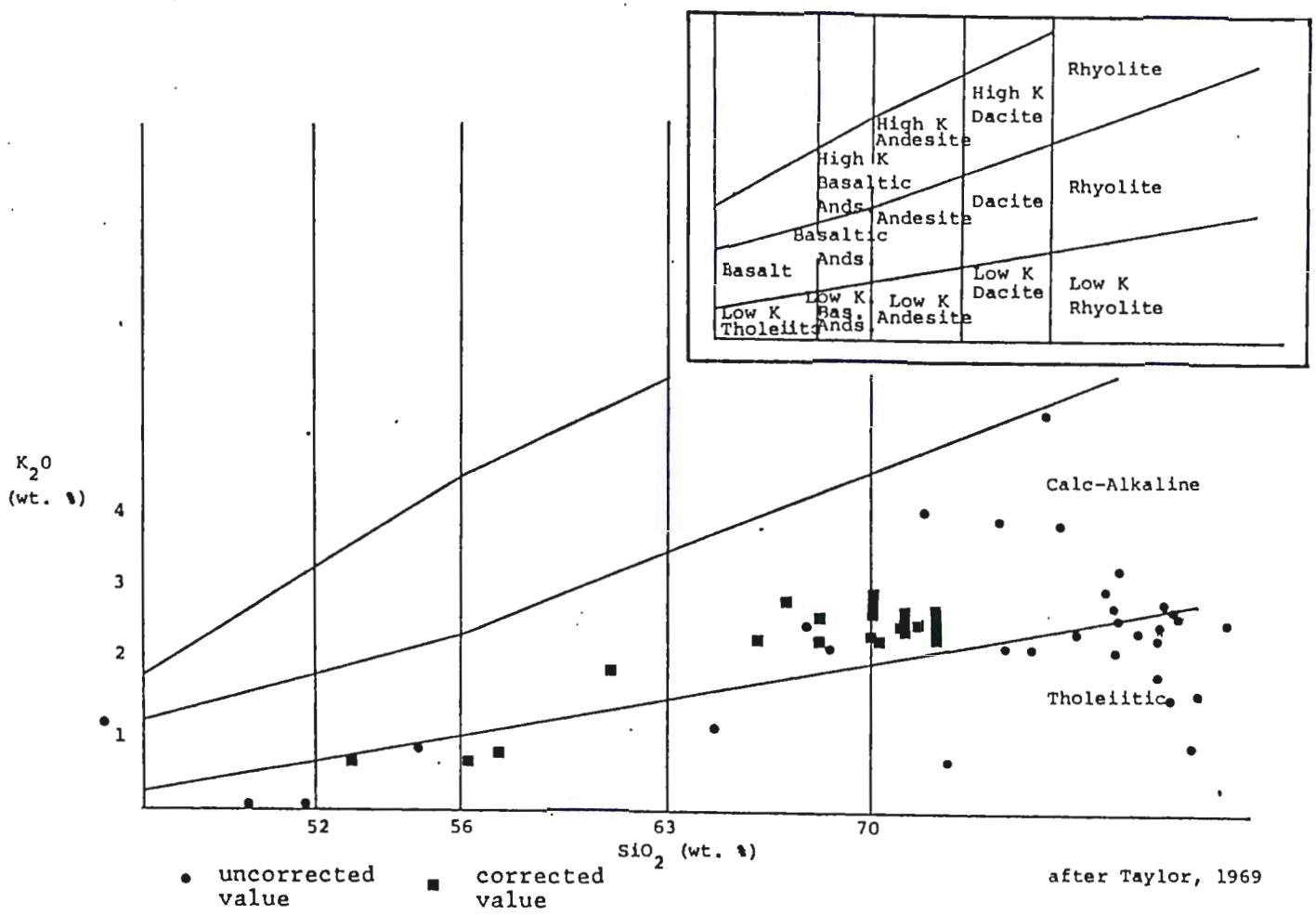
Rhyolite
High K Dacite
High K Andesite
High K Basaltic Ands
Andesite
Basaltic Ands
Dacite
Rhyolite
Basalt
Low K Dacite
Low K Rhyolite
Low K Tholeiite
Low K Bas. Ands
Low K Andesite
$K_2O$ (wt. %)
4
3
2
1
Calc-Alkaline
Tholeiitic
52
56
63
70
$SiO_2$ (wt. %)
• uncorrected value
■ corrected value
after Taylor, 1969

Figure 8

Trace values for twelve minor elements were reported in parts per million (Table 3, Appendix II). Of these twelve elements, four were not used in the various graphs due to: 1) lack of variation in the values (Mo, Cd) and 2) probable contamination of the samples due to the use of a chrome steel mortar and pestle in TSL's laboratory sample preparation procedure (Cr, V).

Figure 9 is a trace element vs. $SiO_2$ variation diagram. It shows good correlation within individual units and generally confirms field and petrographic interpretations made in the previous chapter. Figure 9 also shows depletion of $TiO_2$ and Zr, Co, Ni, and Pb with increasing $SiO_2$ content and increasing Y and Cu with increasing $SiO_2$. The trace elements Zn and Sb do not show any recognizable trends.

Figure 10 shows trace element variation with apparent stratigraphic height in the hope of detecting zonation patterns within the pyroclastic crystal tuff units (Unit 3). Unfortunately, no recognizable zonation patterns were delineated.

Figure 9

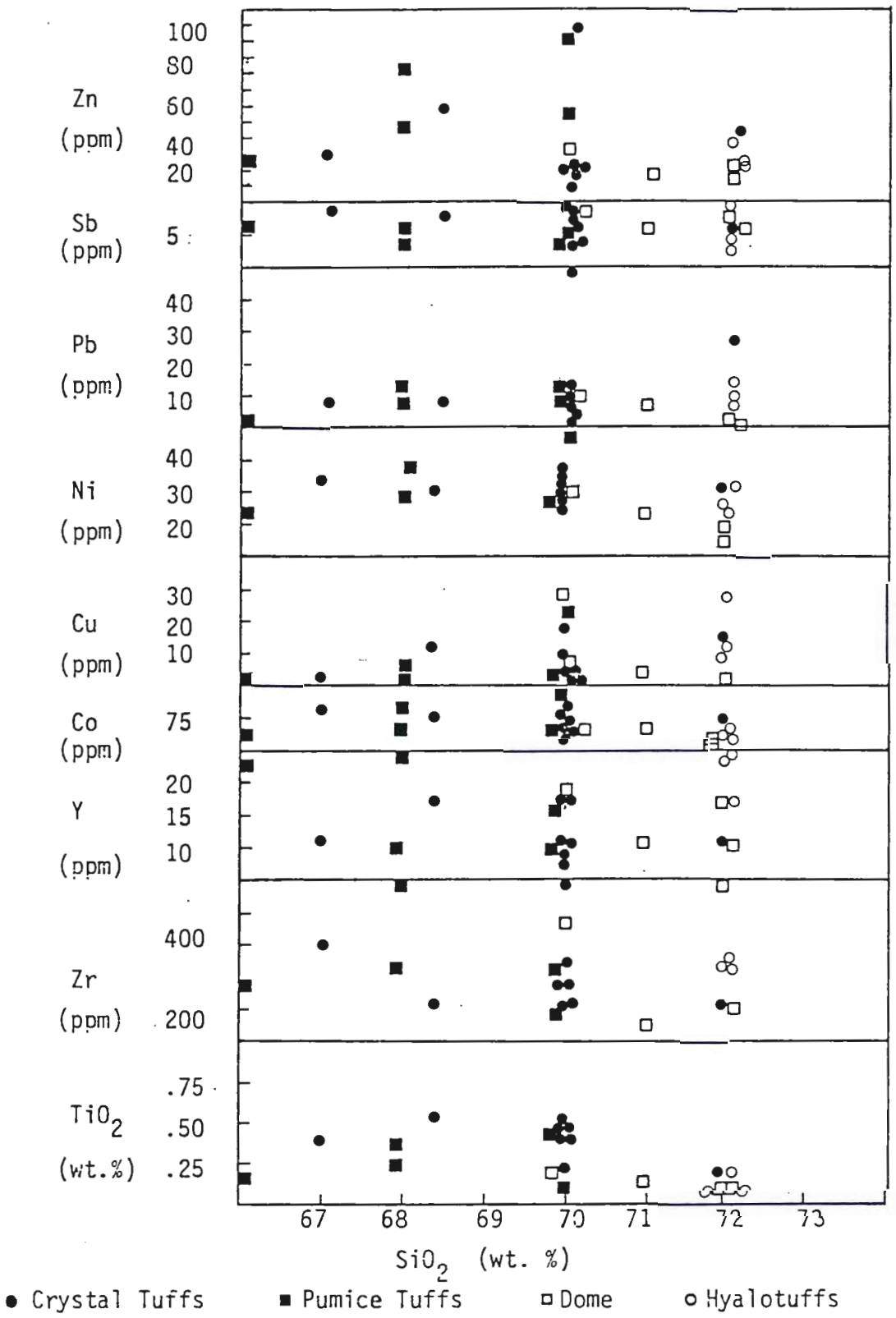
Zn (ppm)
100
80
60
40
20
Sb (ppm)
5
Pb (ppm)
40
30
20
10
Ni (ppm)
40
30
20
Cu (ppm)
30
20
10
Co (ppm)
75
Y (ppm)
20
15
10
Zr (ppm)
400
200
TiO2 (wt.%)
.75
.50
.25
67
68
69
70
71
72
73
SiO2 (wt. %)
● Crystal Tuffs
■ Pumice Tuffs
□ Dome
○ Hyalotuffs

Figure 10

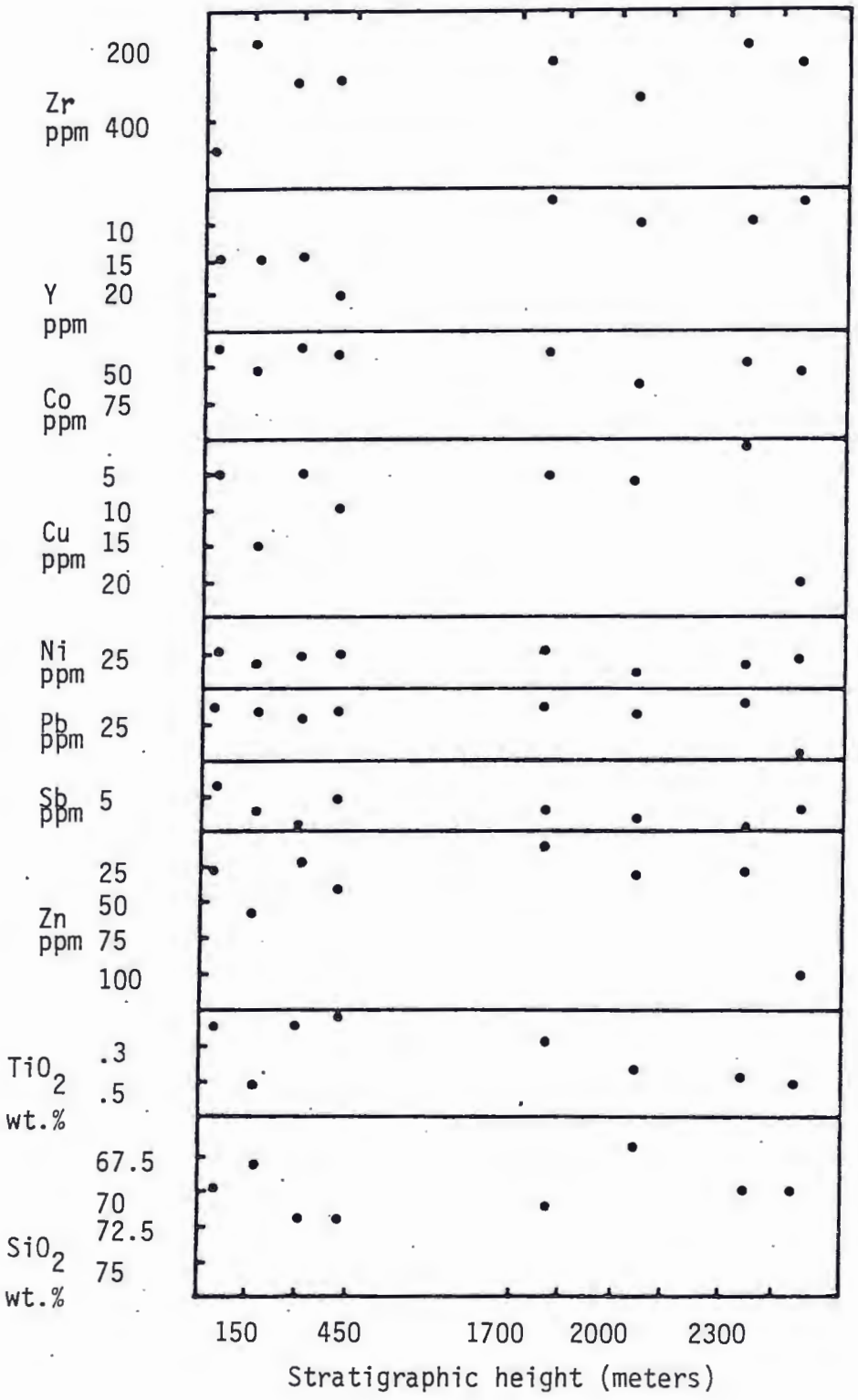
200
Zr ppm 400
10
15
Y 20
ppm
50
Co 75
ppm
5
10
Cu 15
ppm
20
Ni 25
ppm
Pb 25
ppm
Sb 5
ppm
25
50
Zn 75
ppm
100
TiO2 .3
.5
wt.%
67.5
70
72.5
SiO2 75
wt.%
150
450
1700
2000
2300
Stratigraphic height (meters)

# IV: SUMMARY AND CONCLUSIONS

## IV.1 Evidence for Subaqueous Volcanism

The following is a list of observations which support the conclusion that subaqueous volcanism was dominant within the study area:

1) Bedded and graded, pyroclastic flow deposits that pass upward into finely laminated hyalotuffs (upward-fining sequence as described by Fiske and Matsuda, 1964).
2) Symmetrical bomb-sagged bedding feature (Fisher, 1980, personal communication).
3) Accretionary lapilli (Waters and Fisher, 1971; Moore and Peck, 1962).
4) Extensive, nonwelded, crystal tuff sequences that grade upward into pumice-bearing tuff sequences suggesting segregation due to different settling rates of crystal and pumice through a water column (Fiske and Matsuda, 1964).
5) Long-tube pumice (Fiske, 1969).
6) Directly overlying volcanogenic iron formation passing stratigraphically upward into pillowed basalts.
7) Andesite pillow breccias.
8) Association with other subaqueous deposits within the region.

Small portions of the succession may have been produced by subaerial eruptions. These include the andesite flows and the Merapi-type pyroclastic flows.

## IV.2 Summary and Conclusions

The initial stages of felsic volcanism in the map area were short-lived, subaqueous, phreatomagmatic eruptions which produced bedded hydroclastic rocks. Bedded and normally-graded, lithic-rich, pumice-poor, pyroclastic flow deposits were produced from an eruption column containing a high percentage of accessory lithic material. These rocks pass upward into finely bedded hyalotuffs, with accretionary lapilli, which formed when the eruption column contained little or no accessory material.

Alternatively, the bedded pyroclastic flow deposits and hyalotuffs may represent a fining upward sequence (after Fiske and Matsuda, 1964) where the bedded pyroclastics represent the dense fragment portion and the hyalotuffs represent the fine suspended ash portion.

The second stage of felsic volcanism is characterized by the development of a sustained eruption column. Continuous eruption column collapse produced the thick sequences of nonwelded, crystal and pumice-bearing pyroclastic flow deposits. Two possible mechanisms of eruption come to mind: 1) An eruption column breaks out of a subaqueous environment becoming in part subaerial with quenched debris from the eruption column raining down into the sea. The segregation of the crystal tuffs from the pumice tuffs is believed to be the result of density differences, and, therefore, different settling rates of crystals and pumice through a water column thus forming crystal tuffs that pass stratigraphically upward into pumice-bearing tuffs. 2) Subaerial eruption column produces segregated crystal tuffs and pumice-bearing tuffs by the bouying up of pumice by escaping gases within a fluidized pyroclastic flow (Sheridan, 1979).

The total absence of any indication of welding, coupled with the stratigraphic thickness of the crystal tuffs and pumice-bearing tuffs and their spatial association with subaqueous volcanic rocks points to the first alternative as being the most plausible.

The third stage of eruptive activity was another subaqueous, phreatomagmatic episode, much like stage one activity. These bedded, pyroclastic flow deposits and hyalotuffs, however, are interbedded with small andesite lava flows, pillow breccias, and pyroclastic flows that probably originated from volcanic vents that were apparently not related to the vents that produced the rhyolites.

The fourth stage of eruptive activity is represented by a crystal tuff, pumice-bearing tuff sequence emplaced in similar manner to stage two crystal tuff, pumice-bearing tuffs. These crystal tuffs differ, however, in exhibiting a distinct mineralogical zonation from a plagioclase rich bottom to a quartz rich top (with increasing stratigraphic height). This zonation is thought to reflect an original zonation within the magma chamber. The crystal tuffs grade stratigraphically upward into pumice tuffs.

The fifth stage of volcanic activity defined within the area, involved the growth of intrusive-extrusive felsic domes and/or lava flows and related block and ash pyroclastic flow deposits. An early period of dome growth is marked by milky quartz veins within the fragments of the block and ash flows which are terminated at the fragments' edge. Later renewed growth of the dome resulted in the emplacement of block-and-ash and lapilli-and-ash pyroclastic flow or debris flow deposits. The presence of a few percent pumice, similarity of fragments to matrix, and

the lack of weathering rinds on the fragments points to Merapi-type pyroclastic flow, rather than a debris flow origin.

The last stage of felsic volcanism in the area resulted in hot springs and fumeroles that deposited the Helen Iron Formation and altered the footwall rhyolites.

The area was then faulted and possibly folded and metamorphosed to lower greenschist facies.

The last phase of igneous activity, occurring after and/or during the metamorphism and probably after or during the faulting, was the intrusion of the gabbroic dikes.

Pleistocene glaciation modified drainage and topography, and left a mantle of unconsolidated deposits over parts of the region.

## IV.3 Conclusions

Map units established in the field were substantiated by subsequent chemical analyses. On the basis of petrochemistry, petrography, and field characteristics, the felsic metavolcanics are divisible into: 1) subaqueous, phreatomagmatic, bedded, pyroclastic flow deposits and related hyalotuffs, 2) massive crystal-rich and pumice-rich pyroclastic flow deposits, 3) flow laminated, massive, and/or spherulitic intrusions, domes and/or lava flows, and dome collapse pyroclastic flows, and 4) iron formation. The felsic metavolcanics are cut by contemporaneous intermediate metavolcanics and by later mafic dikes or sills.

The felsic metavolcanics were metasomatized and through a metasomatism correction procedure (Beswick and Soucie, 1978) the mobile constituents were identified. Within the thesis area, $SiO_2$ has been added to the felsic volcanic rocks, FeO + MgO, Fm, CaO, and $Na_2O$ depleted, and $K_2O$, in about half the samples has been added and half the samples depleted (Appendix II).

# REFERENCES

Algoma Exploration Ltd., 1980, Company Reports and Maps.

Beswick, A. E., and Saucie, G., 1978, A Correction Procedure for Metasomatism in an Archean Greenstone Belt: Precambrian Research, vol. 6, pp. 235-248.

Coleman, A. P., and Willmott, A. B., 1902, The Michipicoten Iron Ranges: Univ. Toronto Studies, Geologic Series, #2, pp. 1-83.

Collins, W. H., and Quirke, T. T., 1926, Michipicoten Iron Ranges: Geol. Survey Canada Mem. 147, pp. 1-170.

Fisher, R. V., 1980, Personal Communication.

Fiske, R. S., 1969, Recognition and Significance of Pumice in Marine Pyroclastic Rocks: Geol. Soc. America Bull., vol. 80, pp. 1-8.

Fiske, R. S., 1963, Subaqueous Pyroclastic Flows in the Ohanapecosh Formation, Washington: Geol. Soc. America Bull., vol. 74, pp. 391-406.

Fiske, R. S., and Matsuda, T., 1964, Submarine Equivalents of Ash Flows in the Tokiwa Formation, Japan: Amer. Jour. Sci., vol. 262, pp. 76-106.

Gledhill, T. L., 1927, Michipicoten Gold Area, District of Algoma: Ont. Dept. Mines 36th Annual Reports, pt. 2, pp. 1-49.

Goodwin, A. M., 1964, Geochemical Studies at the Helen Iron Range: Econ. Geology, vol. 59, pp. 684-718.

Goodwin, A. M., 1962, Structure, Stratigraphy, and Origin of Iron Formations, Michipicoten Area, Algoma District, Ontario, Canada: Geol. Soc. America Bull., vol. 73, pp. 561-586.

Goodwin, A. M., 1960, Genetic Aspects of Michipicoten Iron Formation: Canadian Inst. Mining and Metallurgy Trans., vol. 64, pp. 32-36.

Goodwin, A. M., Monster, J., and Thode, H. G., 1976, Carbon and Sulfur Isotope Abundances in Archean Iron Formations and Early Precambrian Cite: Econ. Geology, vol. 71, pp. 870-891.

Green, J. C., 1981, Personal Communication: Univ. of Minnesota-Duluth.

Grout, F. F., 1926, Michipicoten Iron Ranges: Econ. Geology, vol. 21, p. 813.

Hughes, C. J., 1972, Spillites, Keratuphyres, and the Igneous Spectrum: Geologic Magazine, vol. 109, #6, pp. 513-527.

Irvine, T. N., and Baragar, W. R. A., 1971, A Guide to the Chemical Classification of the Common Volcanic Rocks: Can. Jour. Earth Sciences, vol. 8, pp. 523-548.

LaTour, T. E., Kerrich, R., Hodder, R. W., and Barnett, R. L., 1980, Chloritoid Stability in Very Iron-Rich Altered Pillow Lavas: Contributions to Mineral Petrol., vol. 74, pp. 165-173.

Marsden, R. W., 1948, The Mildred Iron Range, Michipicoten District, Ontario: Jalore Mining Company Report, pp. 1-16.

Moore, E. S., 1948, Structure of the Michipicoten-Goudreau Area, pp. 414-419 in Structural Geology of Canadian Ore Deposits: Canadian Inst. Mining and Metallurgy, pp. 1-948.

Moore, E. S., 1931, Goudreau and Michipicoten Gold Areas: Ont. Dept. Mines 40th Annual Report, pt. 4, pp. 1-54.

Moore E. S., and Armstrong, H. S., 1946, Iron Deposits in the District of Algoma: Ont. Dept. Mines 55th Annual Report, pt. 4, pp. 1-118.

Moore, J. G., and Peck, D. L., 1962, Accretionary Lapilli in Volcanic Rocks of the Western Continental United States: Jour. Geol., vol. 70, pp. 182-193.

Morton, R. L., 1981, Personal Communication: Univ. of Minnesota-Duluth.

Rupert, R. J., 1975, McMurray Township and Parts of Surrounding Townships, District of Algoma: Ont. Division Mines, Preliminary Map p. 828, Geologic Series, Compilation 1970 to 1972.

Sage, R., 1980, Geologic Maps of Chabanel, Esquega, Castheals and McMurray Townships, District of Algoma: In Progress, Ontario Geologic Survey.

Sage, R., 1980, Personal Communication: Ont. Geol. Survey.

Sangster, D. F., 1972, Precambrian Volcanogenic Massive Sulfide Deposits in Canada: A Review; Geologic Survey of Canada, Paper 72-22, pp. 1-44.

Sheridan, M. F., 1979, Emplacement of Pyroclastic Flows: A Review; in Chapin, C. E., and Elston, W. E., Ash Flow Tuffs: GSA Spec. Pap. 180, pp. 1-211.

Tanton, T. L., 1948, New Helen Mine, pp. 422-429 in Structural Geology of Canadian Ore Deposits: Canadian Inst. Mining and Metallurgy, pp. 1-948.

Taylor, S. R., 1969, Trace Chemistry of Andesites and Associated Calc-Alkaline Rocks: Proceedings of the Andesite Conference, University of Oregon, pp. 43-64.

Wanless, R. K., 1970, Isotopic Age Map of Canada: Geol. Survey Canada, Map 1256A, Scale 1:5,000,000.

Waters, A. C., and Fisher, R. V., 1971, Base Surges and Their Deposits: Capelinhos and Taal Volcanoes: Jour. of Geophy. Research, vol. 76, pp. 5596-5614.

# Appendix I

## Texture and Mode of Representative Metavolcanic Rocks

### Abbreviations

| Textures | Abbreviation |
|---|---|
| Diabasic | D |
| Ophitic | O |
| Accretionary Lapilli | Al |
| Very Fine Grained | V |
| Fine Grained | F |
| Medium Grained | M |
| Coarse Grained | C |
| Blastoporphyritic | Bp |
| Amygdaloidal | Am |
| Fragmental | Fr |
| Flow Laminated | Fl |
| Porphyritic | P |
| Spherulitic | Sp |
| Hypidiomorphic | H |

| Minerals | |
|---|---|
| Plagioclase | Pl |
| Orthoclase | Or |
| Siderite | Si |
| Ankerite | Ank |
| Pyrite | Py |
| Magnetite | Mt |
| Hematite | Ht |
| Ilmenite | Il |
| Leucoxene | Le |
| Stilpnomelane | St |
| Epidote | Ep |
| Zircon | Z |
| Tourmaline | To |
| Biotite | B |
| Hornblende | Hb |

Appendix I

| Number | T.S. | Texture | Quartz | Feldspar | Carbonate | Serecite | Chlorite | Opaque | Chloritoid | Accessory |
|---|---|---|---|---|---|---|---|---|---|---|
| 1 | 22-1 | P,V | 15 | 15 | 14 | 14 | 1 | 1Py | | |
| 2 | 8-9 | Fr,V | 20 | 15 | 40 | 20 | | 5Py | | |
| 3 | 8-1 | Bp,V | 20 | 15 | 20Si | 25 | | | 30 | |
| 4 | 5-8 | V | 18 | 2 | 65 | 10 | | 4Py | | |
| 5 | 2-1 | P,V | 20 | 10 | 10Si | 1 | 9 | 50Mt | | 1St |
| 6 | 7-5 | S,F | 80 | | 3Si | 10 | | 2Mt | | |
| 7 | 5-3 | S,Bp,V | 60 | 10 | 10Si | 4 | | | 15 | 5St |
| 8 | 23-1 | S,Fr,Fl | 44 | 25Pl,25Or | 1Si | 5 | | | | 1Ep |
| 9 | 22-8 | P,V | 75 | 14Or | 3Si | 5 | | 2Le,1Il | | |
| 10 | 8-17 | P,Fl,V | 50 | 20 | | 30 | | | | 1To |
| 11 | 5-7 | Fl,P,V | 80 | 5 | | 10 | | 5Mt | | |
| 12 | 7-4 | V,Bp, | 49 | 25 | | 10 | | 1Mt | 15 | |
| 13 | 4-1 | P,Fl,V | 80 | 10Pl | 2Si | 4 | | 2Py | | 2St |
| 14 | 1-1 | P,V | 40 | 10 | | 49 | | 1Ht | | |
| 15 | 5-1 | P,V,Bp | 62 | 10 | | 3 | | | 15 | 10Ep |
| 16 | 4-3 | P,Fl,Fr | 60 | 10 | 1Si | 25 | | 1Mt | | 3St |
| 17 | 20-10 | Bp,V | 65 | 20 | | 5 | | 1Le | 10 | |
| 18 | 19-5 | P,V | 72 | 20Or | | 5 | | 1Py | 1 | 1Ep |
| 19 | 2-5 | Fr,P,V | 60 | 10Pl | 1Si | 25 | 3 | 1Mt | | |
| 20 | 3-2 | Fr,P,V | 60 | 15 | 10Si | 15 | | | | |
| 21 | 3-3 | Fr,V,P | 60 | 9 | 10Si | 20 | 1 | | | 1St |
| 22 | 3-5 | Fr,V | 60 | 15 | 4Si | 20 | | | | 1St |
| 23 | 22-12 | P,Fr,F | 39 | 40Pl | 10Si | 10 | 1 | 1Mt | | |
| 24 | 22-4 | P,Fr,V | 60 | 23 | 5 | 10 | 1 | 1MT | | |
| 25 | 1-3 | Fr,S,P | 70 | 10Pl | 3Si | 15 | | 1Mt | | 1St |
| 26 | 2-3 | P,Fr,V | 60 | 10Pl | | 10 | 10 | 10Mt | | |
| 27 | 2-7 | Bp,Fr,P | 80 | 10Pl | | 1 | | | 9 | |
| 28 | 3-1 | Bp,Fr,P | 50 | 10 | 3Si | 20 | 2 | | 15 | |
| 29 | 3-6 | P,Fr,V | 70 | 10Pl | 5Si | 10 | 5 | | | |
| 30 | 3-8 | P,Fr,V | 50 | 10 | 2Si | 14 | 20 | 3Py | | |
| 31 | 5-4 | Fr,P,V | 55 | 10 | 15Si | 14 | 2 | 3Ht | | |
| 32 | 8-3 | Fr,P,V | 40 | 10 | 15Si | 30 | | 5Mt | | |
| 33 | 8-5 | V,Fr | 70 | 10 | 1Si | 17 | | | | 1St |

Appendix I (Continued)

| Number T.S. | Texture | Quartz | Feldspar | Carbonate | Serecite | Chlorite | Opaque | Chloritoid | Accessory |
|---|---|---|---|---|---|---|---|---|---|
| 34 8-18 | Fr,P,V | 60 | 20 | 1Si | 15 | | 1Mt,1Py | | 3St |
| 35 15-2 | P,V | 50 | 30 | 10 | 5 | | 2Ht | | 1St |
| 36 24-6 | Fr,V | 60 | 17 | 10 | 10 | 2 | 1Le | | |
| 37 24-7 | P,Fr,V | 64 | 10Pl,10Or | | 15 | 1 | 1Le | | |
| 38 24-9 | Fr,V | 60 | 25Pl | | 10 | 3 | 2Py,1Mt | | |
| 39 11-13 | P,Fr,V | 80 | 10 | 2Si | 8 | | | | |
| 40 24-13 | P,Fr,Al | 60 | 25 | | 10 | 4 | 1Mt | | |
| 41 24-1 | P,V | 60 | 13Pl,15Or | | 5 | 4 | 1Le | | 1St |
| 42 12-12 | P,Fr,V | 50 | 25 | 3Si | 20 | | 2Mt | | |
| 43 5-10 | Bp,Fr,V | 50 | 10 | 1Si | 15 | | 1Mt | 13 | 10St |
| 44 11-6 | P,Fr,V | 60 | 15 | 10 | 10 | | 3Py,2Mt | | |
| 45 11-8 | P,Fr,V | 70 | 20Pl | | 8 | | 2Mt | | |
| 46 12-8 | P,Fr,V | 50 | 18 | 1Si | 30 | | 1Mt | | |
| 47 12-10 | P,V | 45 | 15Pl | 4Si | 35 | | 1Mt | | |
| 48 14-1 | P,V | 70 | 20Pl | 3Si | 5 | | 2Il,1Le | | .1Z |
| 49 14-6 | P,V | 45 | 30Pl,10Or | | 10 | | 2Ht,1Mt | | .1Z |
| 50 25-2 | P,V | 40 | 30Pl,25Or | | 2 | | | | 3B |
| 51 10-7 | P,Fr,V | 50 | 28 | 4Si | 15 | | 3Py | | |
| 52 1-4 | P,Fr,V | 60 | 10Pl | | 20 | 8 | 2Py | | |
| 53 23-4 | P,v | 30 | 40Pl,25Or | | 4 | | 1Py | | |
| 54 6-9 | P,Fr,V | 50 | 30 | 3Si | 17 | | 2Mt | | |
| 55 6-3 | P,Fr,V | 55 | 30Pl | 4Si | 10 | | 1Py | | |
| 56 23-6 | Al,V | 70 | 15 | 4 | | | 1Py | | |
| 57 20-2 | Al,Bp,V | 55 | 15Pl,15Or | 10 | 3 | 2 | | | |
| 58 23-11 | P,Fr,V | 50 | 19 | 25 | 5 | 1 | 1Mt | | |
| 59 20-3 | Fr,V | 50 | 27 | | 20 | 1 | 1Py | 1 | 1St,1To |
| 60 12-1 | P,Fr,V | 50 | 24 | 5 | 20 | | 1Mt | | |
| 61 12-5 | Fr,V | 40 | 20 | 30 | 5 | 2 | 2Mt,1Ht | | |

Appendix I (continued)

| Number T.S. | Texture | Quartz | Feldspar | Carbonate | Serecite | Chlorite | Opaque | Augite | Accessory |
|---|---|---|---|---|---|---|---|---|---|
| 62 12-3 | V | 20 | 20 | 15 | 40 | | 3Mt | | 2St |
| 63 10-18 | Fr,V | 40 | 25 | 8Si | 7 | 20 | | | |
| 64 16-3 | Am,Bp,Fr | 20 | $50An_4$ | 10 | 5 | 10 | | | 1B,1To |
| 65 22-13 | P,Fr,V | 20 | $40Pl^{}$ | 10 | | 30 | 1Mt | | |
| 66 18-2 | S,Fr,V | 70 | 15 | 3Si | 10 | | 1Mt,1Il | | 1St,.1Z,.1To |
| 67 26-3 | P,Fr,V | 20 | 10 | 40Ank | | 30 | | | |
| 68 13-4 | Bp,Fr,V | 40 | 25Pl | 10 | 15 | | 5Py | | 5B |
| 69 14-4 | P,Fr,V | 50 | 10 | | 15 | | 3Py,2Mt | | 20B |
| 70 17-1 | S,Fr,Fl | 60 | 19 | 10Si | 10 | | | | 1Z |
| 71 18-1 | H,F | 10 | 50 | 15Ank | | 20 | 5Le | | |
| 72 22-2 | H,M | 2 | 47 | 30Ank | | 20 | 1Le | | |
| 73 22-7 | M,Bp | 10 | | 50Ank | 18 | 20 | 2Le | | |
| 74 21-2 | H,Bp,F | 10 | 4Pl | 60Ank | | 25 | 1Le | | .1To |
| 75 22-9 | M,H,O | 10 | | | | 20 | 10Le | | |
| 76 10-21 | M,H,O | 5 | 40 | | 5 | 5 | 5Le | | |
| 77 6-5 | F,H,O | 3 | $44An_{44}$ | 2 | | 1 | 3Mt | 45 | 3Hb |
| 78 8-4 | M,H,D | 5 | $45An_{60}$ | | | | 5Il | 40 | 5Hb |
| 79 12-6a | F,H,D,Am | 5 | $50Pl^{}$ | | 5 | | 3Il | 17 | 20B |

Appendix II

Whole Rock and Minor Element Geochemistry

Table 1

Weight Percent Major Oxides

| Analysis T.S. | $SiO_2$ | $Al_2O_3$ | $Fe_2O_3$ | CaO | MgO | $Na_2O$ | $K_2O$ | $TiO_2$ | MnO | $P_2O_5$ | LOI |
|---|---|---|---|---|---|---|---|---|---|---|---|
| 1,1-1 | 80.36 | 11.71 | 0.84 | 0.21 | 0.09 | 1.28 | 2.64 | 0.13 | 0.01 | 0.03 | 0.70 |
| 2,5-1 | 79.58 | 12.00 | 3.77 | 0.06 | 0.32 | 0.44 | 0.93 | 0.13 | 0.15 | 0.06 | 1.03 |
| 3,8-17 | 78.99 | 11.68 | 1.27 | 0.02 | 0.15 | 2.77 | 2.78 | 0.14 | 0.01 | 0.03 | 0.45 |
| 4,8-18 | 77.81 | 11.93 | 1.82 | 0.27 | 0.21 | 2.77 | 2.25 | 0.14 | 0.01 | 0.10 | 0.72 |
| 5,11-13 | 77.88 | 12.78 | 1.87 | 0.26 | 0.50 | 1.23 | 2.73 | 0.52 | 0.01 | 0.10 | 1.49 |
| 6,11-12 | 75.75 | 13.78 | 1.23 | 0.03 | 0.30 | 3.25 | 2.50 | 0.48 | 0.01 | 0.07 | 0.96 |
| 7,12-12 | 76.63 | 13.61 | 1.04 | 0.12 | 0.29 | 2.10 | 3.03 | 0.45 | 0.01 | 0.09 | 0.91 |
| 8,14-6 | 73.68 | 13.43 | 3.32 | 0.34 | 0.29 | 3.49 | 2.32 | 0.44 | 0.08 | 0.10 | 1.33 |
| 9,11-6 | 65.87 | 13.91 | 3.30 | 3.24 | 1.14 | 1.82 | 2.46 | 0.41 | 0.08 | 0.10 | 4.97 |
| 10,14-1 | 71.92 | 14.85 | 1.64 | 0.41 | 0.15 | 8.24 | 0.68 | 0.49 | 0.04 | 0.12 | 0.53 |
| 11,16-5 | 76.83 | 12.72 | 0.67 | 0.52 | 0.52 | 2.74 | 2.22 | 0.28 | 0.02 | 0.03 | 1.55 |
| 12,11-2 | 79.94 | 13.17 | 0.76 | 0.01 | 0.16 | 0.93 | 2.76 | 0.28 | 0.01 | 0.01 | 1.26 |
| 13,15-2 | 78.96 | 9.33 | 1.03 | 1.38 | 0.94 | 2.78 | 1.56 | 0.21 | 0.02 | 0.02 | 2.21 |
| 14,16-3 | 63.67 | 16.61 | 4.33 | 2.43 | 1.67 | 4.82 | 1.17 | 0.49 | 0.07 | 0.14 | 3.29 |
| 15,21-2 | 42.57 | 12.71 | 9.42 | 8.86 | 7.20 | 1.45 | 1.18 | 0.58 | 0.16 | 0.09 | 14.39 |
| 16,25-2 | 70.18 | 13.93 | 3.51 | 0.48 | 0.88 | 3.17 | 4.11 | 0.44 | 0.04 | 0.11 | 0.95 |
| 17,23-1 | 75.35 | 12.60 | 1.86 | 0.15 | 0.30 | 2.83 | 3.96 | 0.18 | 0.03 | 0.06 | 1.08 |
| 18,23-6 | 79.36 | 11.24 | 0.96 | 0.06 | 0.16 | 4.21 | 1.60 | 0.11 | 0.01 | 0.04 | 0.11 |
| 19,24-1 | 78.37 | 12.26 | 1.77 | 0.17 | 0.56 | 0.97 | 2.60 | 0.21 | 0.01 | 0.04 | 1.17 |
| 20,24-6 | 67.47 | 13.01 | 4.26 | 3.68 | 1.66 | 0.91 | 2.66 | 0.54 | 0.09 | 0.11 | 4.49 |
| 21,24-9 | 78.91 | 11.91 | 2.19 | 0.02 | 0.93 | 0.67 | 2.41 | 0.20 | 0.02 | 0.05 | 1.52 |
| 22,24-10 | 73.09 | 14.21 | 2.70 | 0.80 | 1.23 | 0.10 | 4.06 | 0.26 | 0.04 | 0.10 | 1.73 |
| 23,24-13 | 78.69 | 11.38 | 1.65 | 0.65 | 0.96 | 0.27 | 2.80 | 0.11 | 0.04 | 0.03 | 1.95 |
| 24,12-5 | 53.72 | 14.20 | 8.86 | 5.87 | 4.51 | 3.88 | 0.89 | 0.79 | 0.15 | 0.17 | 6.51 |
| 25,23-8 | 78.17 | 11.64 | 1.22 | 0.35 | 0.22 | 3.45 | 1.81 | 0.20 | 0.03 | 0.04 | 0.83 |
| 26,H-23 | 75.44 | 11.95 | 1.70/1.2*2.43 | | 0.06 | 2.28 | 2.29 | 0.20 | 0.09 | 0.03 | 2.34 |
| 27,H-19 | 78.20 | 12.32 | 1.62/.39 | 0.44 | 0.93 | 1.45 | 2.89 | 0.12 | 0.06 | 0.07 | 1.57 |
| 28,H-26 | 78.2 | 12.36 | 1.62/.31 | 0.58 | 0.47 | 3.49 | 2.14 | 0.12 | 0.12 | 0.05 | 0.64 |
| 29,H-95 | 50.5 | 13.64 | 2.32/10.2 | 11.1 | 7.53 | 1.52 | 0.09 | 0.82 | 0.24 | 0.06 | 1.95 |
| 30,H-96 | 75.96 | 13.01 | 1.68/.12 | 0.54 | 0.61 | 0.85 | 5.52 | 0.18 | 0.06 | 0.03 | 1.44 |
| 31,H-99 | 78.34 | 12,42 | 1.45/.00 | 0.78 | 0.49 | 0.93 | 3.43 | 0.10 | 0.07 | 0.01 | 1.97 |
| 32,H-100 | 48.48 | 15.42 | 2.27/9.09 | 11.87 | 7.89 | 1.05 | 0.08 | 0.77 | 0.20 | 0.06 | 2.81 |

* $Fe_2O_3/FeO$ values reported for analyses 26 through 32.

Appendix II: Table 2

Weight Percent Major Oxides Corrected for Metasomatism.

| Analysis T.S. | $SiO_2$ | $Al_2O_3$ | Fm* | CaO | $Na_2O$ | $K_2O$ | $TiO_2$ | Total |
|---|---|---|---|---|---|---|---|---|
| 1, 1-1 | 72 | 11.95 | 4.9 | 4.4 | 4.0 | 2.6 | 0.13 | 99.85 |
| 2, 5-1 | 72 | 12.21 | 4.2 | 4.0 | 4.0 | 2.7 | 0.13 | 99.11 |
| 3, 8-17 | 71 | 11.88 | 4.28 | 4.28 | 4.2 | 2.75 | 0.14 | 98.39 |
| 4, 8-18 | 70 | 12.17 | 5.0 | 4.4 | 3.9 | 2.5 | 0.14 | 97.97 |
| 5, 11-13 | 70 | 12.86 | 4.0 | 4.0 | 4.0 | 2.75 | 0.53 | 97.61 |
| 6, 11-12 | 70 | 14.01 | 4.0 | 4.2 | 4.0 | 2.8 | 0.49 | 99.01 |
| 7, 12-12 | 70 | 13.85 | 4.0 | 4.5 | 4.0 | 2.75 | 0.46 | 99.10 |
| 8, 14-6 | 70 | 13.61 | 4.1 | 4.4 | 3.9 | 2.75 | 0.45 | 98.76 |
| 9, 11-6 | 67 | 14.32 | 4.4 | 4.75 | 3.7 | 3.0 | 0.42 | 97.17 |
| 10,14-1 | 70 | 14.99 | 4.2 | 4.7 | 4.0 | 3.0 | 0.49 | 98.89 |
| 11,16-5 | 72 | 12.97 | 4.1 | 4.1 | 4.1 | 2.75 | 0.29 | 100.31 |
| 12,11-2 | 71 | 13.26 | 4.0 | 4.4 | 4.2 | 2.75 | 0.28 | 99.61 |
| 13,15-2 | 66 | 9.48 | 5.5 | 4.7 | 5.5 | 2.5 | 0.21 | 93.68 |
| 14,16-3 | 70 | 16.87 | 5.6 | 7.1 | 3.5 | 2.4 | 0.50 | 105.47 |
| 15,21-2 | 61 | 12.99 | 10.3 | 7.0 | 4.0 | 2.0 | 0.59 | 97.29 |
| 16,25-2 | 69 | 14.27 | 5.0 | 5.0 | 4.0 | 2.5 | 0.45 | 98.77 |
| 17,23-1 | 70 | 12.81 | 4.5 | 4.5 | 3.9 | 2.5 | 0.76 | 98.21 |
| 18,23-6 | 72 | 11.49 | 4.5 | 4.0 | 4.3 | 2.75 | 0.11 | 99.04 |
| 19,24-1 | 70 | 12.49 | 5.2 | 4.4 | 4.0 | 2.5 | 0.21 | 98.59 |
| 20,24-6 | 68.39 | 13.19 | 3.72 | 3.73 | 5.0 | 2.7 | 0.55 | 96.73 |
| 21,24-9 | 72 | 12.06 | 4.0 | 4.0 | 4.2 | 2.7 | 0.20 | 98.96 |
| 22,24-10 | 68 | 14.47 | 4.25 | 5.0 | 4.0 | 2.75 | 0.26 | 98.47 |
| 23,24-13 | 72 | 11.55 | 4.5 | 4.0 | 4.2 | 2.75 | 0.11 | 99.0 |
| 24,12-5 | 56 | 14.36 | 10.55 | 10.0 | 3.92 | 0.80 | 0.80 | 95.63 |
| 25,23-8 | 72 | 11.87 | 4.4 | 4.0 | 4.0 | 2.5 | 0.20 | 98.77 |
| 26,H-19 | 71 | 12.32 | 4.0 | 4.3 | 4.0 | 2.75 | 0.20 | 98.37 |
| 27,H-23 | 71 | 11.95 | 3.6 | 4.0 | 4.1 | 2.7 | 0.20 | 97.35 |
| 28,H-26 | 71 | 12.36 | 4.0 | 4.1 | 4.1 | 2.7 | 0.12 | 98.26 |
| 29,H-95 | 52 | 13.64 | 17.73 | 11.1 | 2.02 | 0.80 | 0.81 | 97.47 |
| 30,H-96 | 70 | 13.01 | 4.2 | 4.3 | 4.1 | 2.7 | 0.17 | 98.31 |
| 31,H-99 | 71 | 12.42 | 4.2 | 4.2 | 4.3 | 2.7 | 0.10 | 98.82 |
| 32,H-100 | 57 | 15.42 | 11.0 | 11.0 | 2.4 | 0.80 | 0.76 | 97.62 |

Fm*=FeO + MgO.

Appendix II: Table 3

Minor Elements (ppm).

| Analysis T.S. | Cd | Co | Cr | Cu | Ni | Mo | Pb | Sb | V | Zn | Zr | Y |
|---|---|---|---|---|---|---|---|---|---|---|---|---|
| 1, 1-1 | 1 | 29 | 192 | 1 | 20 | 1 | 5 | 6 | 3 | 15 | 500 | 15 |
| 2, 5-1 | 1 | 26 | 830 | 2 | 16 | 1 | 14 | 8 | 26 | 20 | 200 | 10 |
| 3, 8-17 | 1 | 45 | 227 | 6 | 23 | 1 | 15 | 6 | 30 | 19 | 150 | 10 |
| 4, 8-18 | 1 | 43 | 294 | 6 | 27 | 1 | 17 | 4 | 9 | 52 | 300 | 15 |
| 5, 11-13 | 1 | 52 | 367 | 20 | 27 | 1 | 48 | 7 | 53 | 101 | 250 | 10 |
| 6, 11-12 | 1 | 46 | 218 | 1 | 31 | 1 | 9 | 9 | 60 | 28 | 200 | 10 |
| 7, 12-12 | 1 | 45 | 227 | 2 | 25 | 1 | 10 | 4 | 48 | 22 | 200 | 10 |
| 8, 14-6 | 1 | 47 | 770 | 10 | 29 | 1 | 20 | 10 | 58 | 28 | 250 | 10 |
| 9, 11-6 | 1 | 59 | 840 | 3 | 36 | 1 | 18 | 8 | 78 | 31 | 350 | 10 |
| 10,14-1 | 1 | 55 | 300 | 2 | 33 | 1 | 14 | 8 | 54 | 26 | 300 | 15 |
| 11,16-5 | 1 | 57 | 191 | 2 | 35 | 1 | 19 | 7 | 25 | 23 | 250 | 10 |
| 12,11-2 | 1 | 37 | 210 | 1 | 20 | 1 | 11 | 7 | 22 | 11 | 250 | 10 |
| 13,15-2 | 1 | 42 | 286 | 3 | 24 | 1 | 9 | 6 | 13 | 28 | 250 | 20 |
| 14,16-3 | 1 | 70 | 1080 | 26 | 47 | 1 | 20 | 5 | 224 | 95 | 200 | 10 |
| 15,21-2 | 1 | 77 | 2240 | 107 | 113 | 1 | 20 | 8 | 880 | 106 | 10 | 10 |
| 16,25-2 | 1 | 61 | 930 | 6 | 38 | 1 | 21 | 6 | 65 | 38 | 300 | 10 |
| 17,23-1 | 1 | 45 | 353 | 8 | 29 | 2 | 18 | 8 | 4 | 31 | 400 | 15 |
| 18,23-6 | 1 | 46 | 236 | 10 | 29 | 1 | 17 | 4 | 4 | 22 | 300 | 25 |
| 19,24-1 | 1 | 38 | 292 | 6 | 24 | 1 | 12 | 4 | 16 | 28 | 500 | 15 |
| 20,24-6 | 1 | 52 | 920 | 13 | 33 | 1 | 16 | 7 | 186 | 58 | 200 | 15 |
| 21,24-9 | 1 | 38 | 368 | 4 | 25 | 1 | 21 | 9 | 26 | 21 | 300 | 15 |
| 22,24-10 | 1 | 48 | 426 | 3 | 31 | 1 | 16 | 4 | 10 | 79 | 600 | 25 |
| 23,23-13 | 1 | 39 | 406 | 11 | 24 | 1 | 14 | 5 | 21 | 40 | 300 | 20 |
| 24,12-5 | 5 | 86 | 2080 | 50 | 118 | 1 | 113 | 9 | 615 | 540 | 100 | 10 |
| 25,23-8 | 1 | 48 | 307 | 18 | 28 | 1 | 37 | 6 | 7 | 43 | 200 | 10 |